Loss of FBXO11 function establishes a stem cell program in acute myeloid leukemia through dysregulation of the mitochondrial protease LONP1

Angela Ya-Chi Mo[1,2], Hayle Kincross[1], Xuan Wang[1], Linda Ya-Ting Chang[1], Gerben Duns[1], Harwood Kwan[1], Tammy Lau[1], T. Roderick Docking[1], Jessica Tran[1], Shane Colborne[1], Se-Wing Grace Cheng[1], Shujun Huang[1], Nadia Gharaee[1], Elijah Willie[1], Jihong Jiang[1], Jeremy Parker[1], Joshua Bridgers[1], Davis Wood[3], Ramon Klein Geltink[2], Gregg B. Morin[1,4], Aly Karsan*[1,2]

[1]Michael Smith Genome Sciences Centre, BC Cancer, Vancouver, British Columbia, Canada.
[2]Department of Pathology and Laboratory Medicine, University of British Columbia, Vancouver, British Columbia, Canada.
[3]Centre for Comparative Medicine, University of British Columbia, Vancouver, British Columbia, Canada.
[4]Department of Medical Genetics, University of British Columbia, Vancouver, British Columbia, Canada.

* Corresponding Author: Aly Karsan, BC Cancer Research Institute
675 West 10th Avenue, Vancouver, British Columbia V5Z 1L3, Canada
Phone: 604.675.8034; e-mail: akarsan@bcgsc.ca

The authors declare that no conflict of interest exists

ABSTRACT

Acute myeloid leukemia (AML) is an aggressive cancer with very poor outcomes. Analysis of sequencing data from 1,727 unique AML patients revealed frequent mutations in ubiquitin ligase family genes. Loss of function of the Skp1/Cul1/Fbox (SCF) E3 ubiquitin ligase complex genes are found in 8 - 9% of adult AML patients including recurrent mutations in *FBXO11*. *FBXO11* is the most significantly downregulated gene of the SCF complex in AML samples. Depletion of *Fbxo11* promotes myeloid-biased stem cell maintenance and cooperates with *AML1-ETO* and mutant *KRAS* to generate serially transplantable mouse and human AML in *in vivo* models. FBXO11 mediates K63-linked polyubiquitination of the LONP1 mitochondrial protease, and loss of *FBXO11* impairs LONP1 activity thereby reducing mitochondrial membrane potential, imparting stem cell properties and driving leukemogenesis. Our findings suggest that loss of FBXO11 function primes HSPC for myeloid-biased self-renewal through attenuation of LONP1-mediated regulation of mitochondrial function.

35 Despite the introduction of new targeted therapies for acute myeloid leukemia (AML), outcomes
36 remain dismal with 5-year survival being <35% overall, and around 10% in those over 60 years old[1].
37 Various sequencing studies have generated molecular classification systems for AML[2,3]. Nevertheless, in
38 a large targeted sequencing study comprising 1,540 AML patients, which established 11 distinct
39 molecular subclasses of AML based on cytogenetic abnormalities and driver mutations, at least 11% of
40 the patients could not be classified into a specific group[3]. Analyses of gene expression studies have
41 suggested that additional genetic, epigenetic and/or clinical parameters play a role in refining genetic
42 classification[2,4].
43 Disruption of the ubiquitin pathway plays an important role in cancer development, as
44 suggested by recurrent genetic aberrations affecting E3 ligases and deubiquitinases in multiple cancers[5–
45 8]. Ubiquitination plays a crucial role in the development and function of normal hematopoietic stem
46 and progenitor cells (HSPC) and leukemic stem cells (LSC)[9–13], but ubiquitin gene mutations do not
47 currently constitute a molecular subclass in AML. Further, although the presence of a ubiquitin pathway
48 mutation has generally been extrapolated to mean that the ubiquitin-proteasome system is
49 defective[8,14,15], results of clinical trials with these inhibitors are conflicting, and suggest that
50 ubiquitination functions independent of proteasome-mediated degradation may play an important role
51 in AML[16].
52 A major issue in molecular characterization of AML is that it is difficult to identify subclasses that
53 are comprised of rare mutations in many different genes across a molecular subclass. We found
54 recurrent somatic mutations affecting multiple components of ubiquitinating enzyme complexes in the
55 AML-Personalized Medicine Project (AML PMP) cohort[2], and confirmed these findings in the Beat AML,
56 TCGA AML, and TARGET AML datasets[17–20]. Using an approach combining mutation analyses and gene
57 expression changes, we identified diminished FBXO11 function – a member of the SKP-CUL-FBox E3
58 ligase family – to be a key aberration imparting LSC function in a subset of AMLs. Loss of *FBXO11*
59 function was evidenced by truncating mutations or copy number loss, and reduced gene expression in
60 AML compared to normal HSPC. Our analyses show that *FBXO11* depletion cooperates with other
61 mutations to induce myeloid malignancy in mouse and human xenograft models. *FBXO11* depletion
62 induces a myeloid-biased quiescent stem cell phenotype by regulating mitochondrial metabolism
63 through K63-linked ubiquitination of the mitochondrial protease, LONP1.
64

65 **RESULTS**

66

67 **Ubiquitin pathway mutations are frequent and mutually exclusive in AML cells**

68 We analyzed RNA-seq data from the AML PMP dataset[2] to identify novel recurrent mutation
69 classes that contribute to the initiation or maintenance of AML. In addition to single nucleotide variants
70 (SNVs) and insertion and/or deletion mutants (indels) in previously described molecular subclasses of
71 AML, we identified SNVs and indels in ubiquitin pathway genes in 11.4% (16/140) of the AML PMP
72 cohort (Supplementary Fig. 1, Supplementary Table 1)[3,21]. Extending the cohort to include AML PMP,
73 TCGA, and Beat AML datasets for a total of 1062 adult AML patients revealed ubiquitin pathway gene
74 mutations in 119 patients (11.2%) (Fig. 1a, Supplementary Table 1). In contrast, only 4.5% (30/665) of
75 pediatric AML patients had ubiquitin pathway mutations (Fig. 1a, Supplementary Table 1). The vast
76 majority of AMLs with ubiquitin pathway system mutations only had one mutation, consistent with
77 mutual exclusivity (Fig. 1a), and suggesting a potential common functional effect of these mutations.
78 Loss-of-function mutations including truncating mutations and copy number loss of the *FBXO11* gene
79 and other members of the Skp1-Cul1-Fbox (SCF) E3 ubiquitin ligase complex were identified in 8.6%
80 (91/1062) of adult AML patients (Supplementary Fig. 1, Fig. 1a). Although there is evidence that
81 deregulated ubiquitination plays a role in leukemogenesis[8,22], the current findings implicate ubiquitin
82 pathway mutations as being an independent and distinct molecular class in AML (Fig. 1a).

83

84 **Haplodeficiency of *FBXO11* promotes the maintenance of primitive cells with myeloid bias**

85 To understand the implications of aberrant ubiquitination, we focused on the recurrently
86 mutated *FBXO11* gene, which encodes the substrate-recognition component of the SCF^{FBXO11} E3
87 ubiquitin ligase complex. *FBXO11* variants occur in 1.8% of non-AML cancers in the TCGA dataset
88 (Supplementary Fig. 2a, Supplementary Table 3). Of the 11 patients with *FBXO11* mutations, 2 patients
89 had a truncating or frame-shift mutation and 7 patients had a single copy deletion (Supplementary Fig.
90 2b), suggesting haploinsufficiency of *FBXO11* in AML. Consistent with loss-of-function mutations, AML
91 samples with *FBXO11* mutations or deletions had lower *FBXO11* transcript expression than wild-type
92 cases (Supplementary Fig. 2c). To determine whether *FBXO11* expression was regulated in AML
93 independent of genomic variants, we compared transcript expression of SCF genes in normal $CD34^+$
94 HSPC and in AML cells. Of all SCF genes, *FBXO11* was the most significantly downregulated in AML
95 samples compared to normal $CD34^+$ HSPC (Fig. 1B and C, Supplementary Table 2). Accordingly, FBXO11

96 protein expression was less than 10% of the level expressed in the K562 cell line in 5/7 of the myeloid
97 cell lines tested (Supplementary Fig. 2d).
98 To determine the effects of *FBXO11* depletion on human hematopoiesis, we analyzed RNA
99 expression of human cord blood-derived $CD34^+$ HSPC lentivirally transduced with a short-hairpin
100 (sh)RNA targeting *FBXO11 (*sh*FBXO11*) or a non-targeting shRNA (shCTR). Depletion of *FBXO11* in human
101 $CD34^+$ HSPC resulted in enrichment of HSC and LSC signatures and diminishment of progenitor cell and
102 heme metabolism signatures compared to control (Fig. 2a, Supplementary Fig. 3a). Liquid culture of
103 $CD34^+$ HSPC resulted in increased $CD34^+$ cell proportions with *FBXO11* knockdown compared to control
104 (Fig. 2b). As absolute cell numbers of $CD34^+$ cells were lower in sh*FBXO11*- than shCTR-transduced cells
105 (Fig. 2b), we postulated that *FBXO11* knockdown promoted quiescence as seen in dormant long-term
106 stem cells. Cell cycle analysis confirmed that *FBXO11* depletion increased the G_0 fraction in the $CD34^+$
107 population (Fig. 2c). Interestingly, although increased in the bulk cultured population of sh*FBXO11* cells,
108 cell death was attenuated in the $CD34^+$ fraction (Supplementary Fig. 3b), suggesting a protective effect
109 of *FBXO11* depletion in HSPC.
110 To verify a role for *FBXO11* depletion in supporting a stem cell phenotype, we examined the
111 immunophenotype of cultured primary $CD34^+$ HSPC exhibiting functional short-term and long-term stem
112 cell ($CD45RA^-$) or progenitor cell ($CD90^-CD45RA^-$) markers[23]. *FBXO11* depletion increased the stem cell-
113 like population, at the expense of the progenitor-like population (Fig. 2d, Supplementary Fig. 3c). In this
114 culture system, all $CD34^+$ cellular subpopulations showed an increase in the G_0 fraction, consistent with
115 *FBXO11* depletion inducing quiescence as found in the total $CD34^+$ population (Fig. 2c, Supplementary
116 Fig. 3d).
117 To examine cell output in *FBXO11*-depleted cells, we cultured $CD34^+$ HSPC following knockdown
118 of *FBXO11*. Following 7 days in liquid culture *FBXO11*-depleted cells displayed myeloid-biased output
119 with expansion of $CD15^+$ myeloid cells, but reduction in erythroid (CD71/CD235a) and megakaryocytic
120 (CD41/CD61) populations compared to control (Fig. 2e). *FBXO11* knockdown resulted in reduced primary
121 colony forming cell (CFC) counts (Fig. 2f), with increased clonogenic activity on secondary replating (Fig.
122 2g), consistent with activation of a quiescent HSPC population. In primary CFC assays, there was
123 significant reduction of erythroid colonies in keeping with the reduced heme metabolism gene
124 expression signature and reduced erythroid differentiation in liquid culture (Fig. 2a, e), and consistent
125 with a previous report demonstrating a role for FBXO11 in erythropoiesis[24]. Together these results

126 suggest that *FBXO11* depletion in human CD34$^+$ cells results in a quiescent myeloid-biased primitive
127 hematopoietic population with stem cell characteristics.
128
129 **_Fbxo11_ depletion cooperates with _AML1-ETO_ to generate serially transplantable mouse leukemia**

130 One sample with an *FBXO11* mutation had a cooccurring *AML1-ETO* (*RUNX1-RUNX1T1*) fusion
131 (Fig. 1a). Since expression of the *AML1-ETO* fusion gene is common in leukemia but not sufficient in
132 isolation to generate murine leukemia[25], we examined whether *FBXO11* depletion would cooperate with
133 *AML1-ETO* to drive leukemogenesis[26]. Mouse bone marrow HSPC were co-transduced with human
134 *AML1-ETO* and sh*Fbxo11*, and transplanted into lethally irradiated mice. Marrow HSPC expressing *AML1-*
135 *ETO* with control shRNA (shLuc), sh*Fbxo11* with empty vector (MIG), or shLuc with MIG were included as
136 controls (Supplementary Fig. 4a). Mice reconstituted with HSPC expressing sh*Fbxo11* with *AML1-ETO*
137 developed myeloid leukemia, with reduced leukemia-free survival compared to mice reconstituted with
138 HSPC expressing *AML1-ETO* alone (median survival of 164 vs 280 days, respectively) (Fig. 3a).
139 At endpoint, *AML1-ETO*/sh*Fbxo11* transplanted mice exhibited leukocytosis, anemia,
140 thrombocytopenia and splenomegaly (Supplementary Fig. 4b) with significant expansion of the Lin$^-$Kit$^+$
141 (LK) myeloid progenitor population in the peripheral blood (Fig. 3b), and increased leukemic blasts in the
142 bone marrow and peripheral blood (Fig. 3c, Supplementary Fig. 4c). Further, *AML1-ETO*/sh*Fbxo11* mice
143 had significant expansion of an immunophenotypic long-term reconstituting hematopoietic stem cell
144 (LT-HSC)-like population compared to the three other control groups (Fig. 3d, Supplementary Fig. 5).
145 Serial transplantation of bone marrow harvested from *AML1-ETO*/sh*Fbxo11* mice resulted in more
146 aggressive secondary leukemias, consistent with expansion of an LSC population (Fig. 3e). Thus, while
147 neither sh*FBXO11* nor *AML1-ETO* alone was sufficient to generate acute leukemia, the combination of
148 *AML1-ETO* with depletion of *Fbxo11* initiated and maintained murine myeloid leukemias.
149
150 **_FBXO11_ depletion cooperates with _AML1-ETO_ and _KRAS_^{G12D} to generate human myeloid leukemia**

151 Previous studies have shown that the combination of *AML1-ETO* with mutant *RAS* is not
152 sufficient to transform human CD34$^+$ cells, and to-date there is no known combination of mutants with
153 *AML1-ETO* that results in human leukemia[27]. As ubiquitin pathway mutations cooccur with *RAS*
154 mutations (Fig. 1a, Supplementary Fig. 6), we asked whether the combination of *AML1-ETO*, activated
155 KRAS and *FBXO11* depletion could initiate human leukemia. We transduced CD34$^+$ cells with
156 combinations of these variants, and expanded the cells in long-term culture followed by

157 xenotransplantation into NOD.*Rag1*$^{-/-}$;*γc*^{null} (NRG) mice expressing human *IL3*, human *GMCSF*, and
158 human *SCF* (NRG-3GS). CD34^{+} cells were transduced with empty vector (EV), *FBXO11* shRNA (F), K
159 *KRAS*^{G12D} (K), AML1-ETO (A), F+A (FA), F+K (FK), K+A (KA), or all three (FKA), and flow-sorted for the co-
160 expressed fluorescent markers (Fig. 4a).

161 Following long-term co-culture, *FBXO11* knockdown resulted in reduced cell numbers, but
162 significant enrichment of the proportion of CD34^{+} cells when combined with A or KA relative to
163 corresponding controls (Fig. 4b, Supplementary Fig. 7a). Only the combination of all three genetic
164 perturbations (FKA) permitted progenitor readout in CFC assays (Supplementary Fig. 7b).
165 Xenotransplantation of EV, KA, and FKA cells into NRG-3GS mice resulted in significantly reduced overall
166 survival in FKA mice (Fig. 4c). However, of the mice that survived, those with transplanted FKA cells had
167 significantly longer and higher human hematopoietic reconstitution compared to KA- and EV-
168 transplanted mice, suggesting that *FBXO11* knockdown improves long-term *in vivo* repopulating ability
169 of human HSPC (Fig. 4d, Supplementary Fig 8).

170 Morphological examination at endpoint revealed blast cells in the bone marrow, and
171 leptomeningeal infiltration with primitive myeloid cells, consistent with myeloid leukemia (Fig. 4e,
172 Supplementary Fig. 9a, b). FKA mice had significantly increased human hematopoietic cell reconstitution
173 in the spleen and bone marrow, >98% of which were CD33^{+} myeloid cells (Fig. 4f-h, Supplementary Fig.
174 10a). FKA-transplanted mice also had greater numbers of CD34^{+} bone marrow cells at endpoint (Fig. 4i,
175 Supplementary Fig. 10b). Human CD34^{+} cell output post-transplant per initial CD34^{+} cell placed in long-
176 term culture revealed ~6,000-fold expansion of FKA HSPC, while KA HSPC did not result in CD34^{+} cell
177 expansion (Supplementary Table 4, Supplementary Fig. 10c).

178 Serial marrow transplantation resulted in enhanced reconstitution of human hematopoietic
179 populations with FKA cells compared to controls, indicating maintenance or expansion of self-renewing
180 hematopoietic cells (Fig. 4j). Taken together, these results demonstrate that *FBXO11* depletion improves
181 long-term *in vivo* human cell reconstitution, consistent with induction of a myeloid-skewed, long-term
182 self-renewing stem cell state that cooperates with *KRAS*^{G12D} and *AML1-ETO* to generate myeloid
183 malignancy.

184

185 **FBXO11-mediated ubiquitination positively regulates LONP1 mitochondrial function.**

186 To identify substrates of the SCF^{FBXO11} complex, we immunoprecipitated FLAG-tagged FBXO11
187 (FLAG-*FBXO11*) in the presence or absence of endonuclease treatment, and identified 5 common

188 coimmunoprecipitating proteins using tandem mass spectrometry, including components of the
189 SCF^{FBXO11} complex, SKP1, CUL1 and FBXO11 (Fig. 5a). Additional proteins included the mitochondrial
190 protease, LONP1, and the transcriptional repressor THAP5 (Fig. 5a, Supplementary Fig. 11). FBXO11
191 interaction with LONP1 was confirmed by reciprocal co-immunoprecipitation and western blotting
192 (Supplementary Fig. 12), but we were not able to confirm FBXO11 interaction with THAP5. Dysregulation
193 of LONP1 has been associated with colon cancer and melanoma, but has not been studied in the context
194 of AML[28–30].
195 Surprisingly, LONP1 protein abundance was not affected by *FBXO11* depletion or
196 overexpression, suggesting that LONP1 is not targeted by SCF^{FBXO11} for proteasomal degradation (Fig.
197 5b). If FBXO11 acts to activate rather than degrade LONP1, depletion of LONP1 should recapitulate the
198 functional effects of FBXO11 depletion. Indeed, *LONP1* depletion had a similar effect as *FBXO11*
199 depletion on primary $CD34^+$ HSPC differentiation, causing a reduction in the $CD41^+CD61^+$ megakaryocytic
200 and $CD71^+CD235a^+$ erythroid populations, and an increase in the $CD14^+$ and $CD15^+$ myeloid populations
201 (Fig. 5c), supporting a model of FBXO11 activating LONP1.
202 LONP1 is a mitochondrial protease and chaperone protein that has been reported to target
203 misfolded subunits of ETC complex II and complex V for degradation[31]. Consequently, *LONP1* loss
204 reduces oxygen consumption rate and mitochondrial membrane potential (MMP)[30,31]. LT-HSCs and
205 $CD34^+$ HSPC with greater reconstitution potential have reduced MMP, and the disruption of MMP
206 promotes self-renewal in HSCs[32–34]. This is consistent with our data showing that *FBXO11* depletion
207 promotes a stemness phenotype. *LONP1* knockdown reduced MMP, as did *FBXO11* knockdown in 2
208 myeloid cell lines as well as primary $CD34^+$ HSPC (Fig. 5d). Lower MMP was not accompanied by a
209 reduction in mitochondrial mass, suggesting a defect in the electron transport chain (ETC), which is
210 responsible for maintaining MMP (Supplementary Fig. 13). Concordant with this hypothesis, a lower
211 basal respiration rate was observed in *FBXO11*-KO cells compared to *FBXO11*-KO cells reconstituted with
212 wild-type (WT) FLAG-FBXO11 (Supplementary Fig. 14). In contrast, overexpression of WT FLAG-*FBXO11*,
213 but not an F-box domain mutant (ΔFbox-FBXO11) which does not interact with LONP1, increased MMP
214 as expected (Fig. 5e, Supplementary Fig. 15). Thus, FBXO11 interaction with its target protein, LONP1, is
215 necessary for regulating mitochondrial function. To address whether *LONP1* expression is required for
216 FBXO11 functional effects, we combined *LONP1* knockdown with enforced FLAG-*FBXO11* expression.
217 The increase in MMP from FLAG-*FBXO11* expression was blocked by *LONP1* knockdown, indicating that

218 LONP1 is required for mitochondrial regulation by FBXO11 and that LONP1 functions downstream of
219 FBXO11 (Fig. 5f).
220 We next considered potential activating functions of SCF^{FBXO11} as an E3 ubiquitin ligase complex,
221 or an E3 NEDD8 ligase complex[35,36]. Although K63-linked polyubiquitination activity has not previously
222 been reported for this complex, we immunoprecipitated LONP1 and blotted for K63-linked
223 polyubiquitination and NEDD8. FLAG-*FBXO11* expression increased both K63-linked polyubiquitination
224 and neddylation of LONP1 (Fig. 5g, h), consistent with the potential for FBXO11 having an activating
225 effect on LONP1, mediated through either one or both of these modifications.
226 In order to determine whether ubiquitination or neddylation is responsible for LONP1 activation
227 by FBXO11, K562 cells were lentivirally transduced to express FLAG-*FBXO11* to increase basal MMP
228 levels, and then treated with ubiquitin activating enzyme or NEDD8-activating enzyme inhibitors to
229 determine if either mimicked the effect of *FBXO11* depletion. Only treatment with ubiquitin- but not
230 NEDD8-activating enzyme inhibitors resulted in reduced MMP as observed with *FBXO11* knockdown
231 (Fig. 5i). As would be predicted, proteasome inhibitors also did not reduce FBXO11-mediated MMP
232 elevation, implicating FBXO11-mediated activating ubiquitination of LONP1, rather than proteasomal
233 degradation in regulating its mitochondrial function (Fig. 5j).
234
235 **Transcriptomic trends are consistent with a model of FBXO11 activating LONP1 to regulate stem cell**
236 **maintenance.**
237 As an alternate approach to confirm that FBXO11 regulates LONP1 function, we performed RNA-
238 seq on primary $CD34^+$ HSPC expressing combinations of shRNAs targeting *FBXO11* or *LONP1* alone, or
239 combined with enforced *LONP1* or FLAG-*FBXO11* expression (Supplementary Fig. 16). Analysis of the
240 samples based on Euclidean distances clustered *LONP1* overexpressing samples with control conditions
241 (Fig. 6a), suggesting that overexpression of LONP1 is not sufficient for increased activity, and likely
242 requires activation, potentially by FBXO11. Similarly, *FBXO11* knockdown samples (shFBXO11_9) also
243 clustered closely with samples with *FBXO11* knockdown and *LONP1* overexpression (shFBXO11_LONP1),
244 suggesting that LONP1 overexpression cannot reverse the phenotype generated by depletion of
245 *FBXO11*. Principal component analysis (PCA) confirmed the findings that LONP1 overexpression was not
246 sufficient to alter gene expression, but knockdown of LONP1 inhibited the transcriptional response
247 evoked by FBXO11 overexpression (Supplementary Fig. 17).

248 Given that *FBXO11* depletion results in a stem cell phenotype, and *FBXO11* and *LONP1* depletion
249 result in reduced mitochondrial activity, we performed Gene Set Enrichment Analysis (GSEA) to confirm
250 that the HSC and mitochondrial functional effects initiated by *FBXO11* depletion are dependent on loss
251 of LONP1 function. Both *FBXO11* and *LONP1* knockdown positively enriched for HSC/LSC gene sets (Fig.
252 6b). FLAG-*FBXO11* expression had the opposite effect with reduced expression of genes in the HSC-LSC
253 gene set, while constitutive *LONP1* expression had a negligible effect. *LONP1* depletion blocked the
254 effect of FLAG-*FBXO11* overexpression, indicating that FBXO11-mediated loss of stemness is mediated
255 by LONP1. These results further support the role of LONP1 as a mediator of FBXO11-driven loss of stem
256 cell characteristics. Similar trends were present in HSC and mitochondrial respiratory chain defect gene
257 sets, which were enriched in upregulated genes with *FBXO11* and *LONP1* knockdown and
258 overrepresented in the downregulated genes with constitutive *FBXO11* expression, while *LONP1*
259 knockdown reversed or blocked the effect of *FBXO11* expression (Fig. 6c). Accordingly, the opposite
260 trend was observed in a progenitor gene set, which was overrepresented in the downregulated genes
261 when *FBXO11* or *LONP1* was knocked down, and enriched in the upregulated genes with *FBXO11*
262 overexpression (Fig. 6c). Consistent with transmitting FBXO11 functions, *LONP1* knockdown blocked the
263 loss of a stem cell signature and mitochondrial effects of enforced *FBXO11* expression (Fig. 6c). These
264 gene expression patterns support a model of *FBXO11* depletion regulating mitochondrial function and
265 stem cell maintenance through reduced LONP1 function.
266 Next, we examined whether *FBXO11* and *LONP1* knockdown enriched for a stem cell
267 transcriptomic state with myeloid bias, as shown based on results from previous experiments. Genes
268 that were upregulated with the knockdown of *FBXO11* and *LONP1* shared similar transcriptomic profiles,
269 with enrichment in genes associated with HSC and myeloid cell populations including common myeloid
270 progenitors (CMP), granulocyte-monocyte progenitors (GMP), myelocytes, and myeloid dendritic cells
271 (mDC) (Fig. 6d). Aligning with these trends, genes downregulated with FLAG-*FBXO11* expression were
272 strongly enriched in HSC, CMP, and GMP associated genes, but when combined with *LONP1* knockdown,
273 this effect was attenuated and the megakaryocyte-erythroid progenitor state was enriched (Fig. 6d, e).
274 The latter aligns with the loss of megakaryocytic and erythroid differentiation with *LONP1* depletion that
275 we observed in HSPC, again demonstrating that *LONP1* expression is required for FBXO11 functional
276 effects. We also noted that the transcriptomic profile of cells with *FBXO11* depletion combined with
277 *LONP1* overexpression highly resembled cells with *FBXO11* depletion alone, further supporting a model
278 of LONP1 function that is dependent on *FBXO11*-mediated regulation (Fig. 6f).
279

280 **DISCUSSION**

281 In this work we highlight ubiquitin pathway mutations as a novel class of AML mutations. We
282 implicate *FBXO11* depletion in leukemogenesis, and identify a novel connection between ubiquitination
283 and mitochondrial function through FBXO11-mediated regulation of the mitochondrial protease and
284 chaperone, LONP1, independent of the proteasome system. Consistent with previously characterized
285 activating effects of K63-linked polyubiquitination of target proteins, our data suggest that FBXO11
286 modification of LONP1 promotes LONP1 mitochondrial function resulting in an increase in MMP. Our
287 results further suggest that FBXO11 ubiquitination of LONP1 is required to activate LONP1 function. This
288 activating effect is in contrast to the few other FBXO11 targets previously reported. For instance,
289 SCF^{FBXO11} has been shown to target BCL6, CRL4, and Snail family transcription factors for ubiquitination
290 and subsequent proteasomal degradation[37–39]. SCF^{FBXO11}-mediated neddylation of p53 also inhibits p53
291 transcriptional activity[35]. Our findings provide an explanation as to why *LONP1* was not detected in a
292 screen for identifying mitochondrial contributors to leukemogenesis, as the readout in that study was
293 reduced leukemia cell viability with target gene knockdown[40]. In our model, it is reduced LONP1 function
294 due to *FBXO11* depletion, not LONP1 activation, that is responsible for leukemogenesis.

295 The RNA-seq expression data support FBXO11 as an upstream regulator of LONP1 and solidify
296 the mitochondrial defect link between *FBXO11* and *LONP1* depletion. The mitochondrial respiratory
297 chain defect geneset expression trends are consistent with the reduced MMP characteristic of
298 functional stem cells we observed with *FBXO11* and *LONP1* depletion. Of interest, the reduction in
299 erythroid differentiation resulting from *LONP1* depletion, which mimicked the effects of *FBXO11*
300 depletion and is also reflected in our transcriptomic data is supported by previous reports on the role of
301 LONP1 in heme biosynthesis[41].

302 Loss of ETC function can result from the accumulation of misfolded ETC proteins shown to occur
303 with *LONP1* loss, or from loss of LONP1 chaperone activity required for proper folding of some ETC
304 proteins[31,42]. We found that both *FBXO11* and *LONP1* depletion reduced MMP, and that FBXO11 acts
305 through regulation of LONP1. LT-HSCs and $CD34^+$ cells that have greater reconstitution potential are
306 both characterized by low MMP[32–34]. Disruption of MMP also promotes self-renewal in HSCs, indicating
307 that low MMP is essential for maintaining an HSC state[34]. Additionally, while *FBXO11* depletion has
308 previously been shown to impart apoptotic effects, our work shows that this is not true for primitive
309 HSPC. Rather, *FBXO11*-depleted HSPC are protected from apoptosis and remain in G_0 of the cell cycle.

310 These findings are also consistent with the stem cell characteristics we observed with *FBXO11* depletion,
311 both functionally, and at the transcriptional level.
312 While mitochondrial metabolism and function in stem cells have recently been a focus in stem
313 cell research, there is no consensus on how exactly reduced mitochondrial function promotes a stem
314 cell state or contributes to leukemogenesis. Metabolic changes and products of metabolic pathways
315 have been shown to impact nuclear transcription as well as chromatin and epigenetic remodeling,
316 particularly in cancers[43,44]. In fact, changes in MMP have previously been shown to affect nuclear gene
317 expression in macrophages, suggesting one mechanism for how reduced mitochondrial function might
318 promote a stem cell state[45].
319 In this work, we suggest that mutations of ubiquitin pathway genes may represent a novel
320 molecular subclass in AML. Further, we demonstrate the leukemogenic effects of *FBXO11* loss. We draw
321 a novel connection between the ubiquitin pathway and the mitochondrial protease system. In
322 particular, we show that LONP1 is a target that is activated, rather than degraded following FBXO11-
323 mediated ubiquitination, and this acts as a regulator of hematopoiesis. Importantly, this work suggests
324 that altered gene expression independent of genetic variants may implicate ubiquitin system gene
325 defects in a much wider cohort of AML patients.
326

327 **METHODS AND MATERIALS**

328 **Mutation calling for oncoprint inclusion**

329 Patient mutations were determined pathogenic and included in the oncoprint if they had a
330 REVEL score > 0.250 and CADD score > 10.5. Germline variants were excluded. Hugo Gene Nomenclature
331 Committee (HGNC) gene data was used to generate a list of ubiquitination genes to query, and the list
332 was manually filtered to retain genes functionally relevant to the UPS. For determining the REVEL score
333 threshold of 0.25 for pathogenicity, data for pathogenic solid tumor variants were obtained from *Cheng*
334 *et al* (Memorial Sloan Kettering-Integrated Mutation Profiling of Actionable Cancer Targets (MSK-
335 IMPACT))[46], and variants that were reported less than five times in the Catalogue of Somatic Mutations
336 in Cancer (COSMIC) were excluded. Pathogenic variants associated with human hematological cancers
337 were obtained from *Jaiswal et al*[47], and variants that were reported less than 5 times in COSMIC were
338 excluded.

339 **Odds ratios calculations**

340 Odds ratios were calculated as "odds of a mutation occurring in a sample with a UPS mutation"
341 vs "odds of a mutation occurring in a sample without UPS mutations".
342 Odd ratio for mutations in gene X=

343 $$\frac{\text{\# patients with mutation in X and at least 1 UPS mutation}}{\text{\# patients with at least 1 UPS mutation}} \Big/ \frac{\text{\# patients with mutation in X and no UPS mutations}}{\text{\# of patients with no UPS mutations}}$$

344 **Isolation of human HSPCs**

345 Human HSPC isolation was performed by the Stem Cell assay core at BC Cancer Research
346 Institute. Anonymized normal human cord blood samples were obtained with informed consent from
347 normal full-term Cesarean section deliveries in accordance with procedures approved by the Research
348 Ethics Board of the University of British Columbia and samples from a single day pooled for further
349 processing. $CD34^+$ HSPCs were obtained at >95% purity from pooled collections using a two-step
350 Rosette-Sep/EasySep human CD34-positive selection kit (STEMCELL Technologies) according to the
351 manufacturer's protocols and/or FACS sorting. CB cells were thawed by dropwise addition into HBSS +
352 10% fetal bovine serum (FBS) supplemented with DNase (100 µg/mL final concentration). $CD34^+$ HSPCs
353 were then seeded into 96-well round bottom plates (cell density at 100,000 (100k) cells/100 µL) and
354 prestimulated in StemSpanTM SFEM (Stem Cell Technologies #09650) supplemented with StemSpan™
355 CC100 (Stem Cell Technologies #02690), 750 nM SR1 (Stem Cell Technologies #72344) and 35 nM
356 UM171(Stem Cell Technologies #72912) overnight.

357 **shRNA constructs and CRISPR clones**

358 K562 control and *FBXO11* knockout CRISPR clones were generated by Dr. Gerben Duns. Guide
359 RNAs (gRNAs) were cloned into the pSpCas9n(BB)-2A-GFP (PX461) plasmid (Addgene #48140) and
360 delivered to parental K562 cells by Amaxa nucleofection using the Amaxa Cell line nucleofector kit V
361 (Lonza VCA-1003). GFP+ transfected cells were single-cell sorted into 96-well plates, expanded. *FBXO11*
362 targeting was confirmed by Sanger sequencing, and FBXO11 depletion was confirmed by western blot.
363 shRNAs used are in the pLKO.1 vector, from the MISSION library, and received from the UBC Centre for
364 High-Throughput Biology, and GFP or mCherry was inserted in place of the puromycin resistance
365 marker. gRNA and shRNA information are listed below. More information for gRNA and shRNA targeting
366 can be found in Appendix Figures A.3 and A.4.

367 ***FBXO11* CRISPR gRNAs**

368 gRNA sequence: AACCACTGTAGGGTTAGCATAGG

369 Target exon: Exon 12/23 (antisense, positive strand)

370

371 **Mouse shRNA**

372 TRC clone ID: TRCN0000238633

373 Target: NM_001081034.1 at 1143-1164

374 Target sequence: AGTCAACTGCAGCCCTATTAT

375

376 **Human shRNAs**

377 shCTR

378 Target sequence: CCTAAGGTTAAGTCGCCCTCGC

379 sh*FBXO11* #9

380 TRC Clone ID: TRCN0000004303

381 Target exon: Exon16/23 (isoform 4 NM_001190274.2)

382 Target sequence: GAGTGCTAGAAGACAATGATA

383

384 sh*FBXO11* #10

385 TRC Clone ID: TRCN0000004304

386 Target exon: Exon 5/23 (of isoform 4 NM_001190274.2)

387 Target sequence: GAGAGTTTCCAGCAGTTGTAT

388

389 shLONP1 #1

390 TRCN0000046793, Exon 11/18 (isoform 1 NM_004793.4)

391 Target sequence: CCAGTGTTTGAAGAAGACCAA

392

393 shLONP1 #3

394 TRCN0000046797 Exon 2/18 (isoform 1 NM_004793.4)

395 Target sequence: CCAGCCTTATGTCGGCGTCTT

396

397 **Retroviral constructs**

398 Mouse shRNAs were cloned into the pSIREN-RetroQ plasmid (Addgene #73666). The *AML1-ETO*
399 overexpression construct was purchased from Addgene (#12431).

400

401 **Lentiviral constructs and transduction**

402 High-titre lentiviral supernatants were produced by transient transfection of 293T/17 cells with
403 second-generation packaging/envelope vectors pRRE (Addgene #12251), pREV (Addgene #115989), and
404 pMD2.g (Addgene #12259) using CalPhosTM mammalian transfection kit (Clontech #631312) and
405 incubated for 16 hours, followed by ultracentrifuge concentration (25,000 rpm for 90 min at 4°C;
406 Beckman SW32Ti rotor).

407 $CD34^+$ HSPCs were transduced in 96-well plates (Thermo ScientificTM #12-565-65) with
408 concentrated lentivirus. After 6 hours of incubation, cells were washed once with PBS and transferred to
409 culture medium (StemSpanTM SFEM with StemSpan™ CC100 to culture medium at a 1 in 100 dilution,
410 750 nM SR1 and 35nM UM171). Following 72-hour ex vivo culture, transduced cells were then isolated
411 by sorting for reporter fluorophore expression from lentiviral constructs on a Fusion sorter (Becton
412 Dickenson) using purity mode.

413

414 ***Ex vivo* cord blood liquid culture for differentiation assay**

415 Transduced cells were sorted into 96-well plates at 10k cells/well into 100 µL in StemSpanTM
416 SFEM supplemented with StemSpan™ CC100, 20 ng/mL recombinant human thrombopoietin (hTPO)
417 (BioLegend #597402), DNase (100 µg/mL final concentration), and antibiotics (pencillin and

418 streptomycin). Cells were incubated in a humidified atmosphere at 37°C in room air supplemented with
419 CO2 to achieve a final concentration of 5%.
420
421 **Cell differentiation analysis**
422 $CD34^+$ HSPCs were harvested from culture and washed with PBS with 2% FBS before staining with
423 antibodies at the dilutions listed in Table 2.1 for 1 hour on ice. Cells were pelleted at 300 x g for 5 min,
424 resuspended in PBS with 2% FBS and 1 µg/mL DAPI, and filtered before flow cytometry analysis.

Antibody target	Fluorochrome	Dilution	Clone	Vendor	Catalogue #
CD34	AF700	1:50	581	BD	561440
CD14	APC-Cy7	1:100	63D3	BioLegend	367108
CD11b	BV510	1:100	ICRF44	BioLegend	301334
CD41	PE	1:100	HIP8	BioLegend	303706
CD61	PE-Cy7	1:100	VI-PL2	BioLegend	336416
CD235a	BV711	1:100	HI264	BD Biosciences	740785
CD71	PerCP-Cy5.5	1:100	CY1G4	BioLegend	334114
CD33	BV510	1:100	WM53	BD	563257
CD15	BV786	1:100	HI98	BD	563838

425
426 **Antibodies for mouse peripheral blood analysis**

Antibody target	Fluorochrome	Dilution	Clone	Vendor	Catalogue #
c-Kit	BV650	1:100	2B8	BD	563399
CD45.2	APC-eFluor780	1:100	104	eBioscience	47-0454-82
CD3	PerCP-Cy5.5	1:300	17A2	BD	560527
CD19	APC	1:500	1D3	BD	561738
GR-1	PerCP-Cy5.5	1:2000	RB6-8C5	BD	561103
CD11b	APC	1:800	M1/70	BD	553312

427
428

429 **Antibodies for mouse bone marrow analysis**

Antibody target	Fluorochrome	Dilution	Clone	Vendor	Catalogue #
GR1	PerCP-Cy5.5	1:240	RB6-85C	BD	552093
Ter119	PerCP-Cy5.5	1:15	TER119	eBioscience	45-5921-82
B220	PerCP-Cy5.5	1:60	RA3-6B2	eBioscience	45-0452-80
CD3	PerCP-Cy5.5	1:30	172A	BD	560527
CD4	PerCP-Cy5.5	1:60	RM4-5	BD	550954
CD8a	PerCP-Cy5.5	1:60	53-6.7	BD	551162
IL7R	PerCP-Cy5.5	1:30	A7R34	eBioscience	45-1271-82
cKit	APC	1:10	2B8	eBioscience	17-11171-83
CD16/32	APC-Cy7	1:30	2.4G2	BD	560541
Sca1	PE-Cy7	1:15	D7	BD	558162
CD45.1	FITC	1:10	A20	eBioscience	A14732
Flk2/Flt3	PE-CF594	1:5	A2F10.1	BD	562537
CD34	Biotin	1:2.5	RAM34	eBioscience	13-0341-85
Streptavidin	BV650	1:30	-	BD	563855

430

431 **Long-term initiating cell (LTC-IC)**

432 Two-three days before cell sorting for long-term co-culture with MS5 feeder cells, frozen and X-
433 ray irradiated feeder cells were thawed via dropwise addition into 9 mL DMEM with 15% FBS (15%
434 DMEM) (Invitrogen, 12100-046). The cell mixture was spun down at 300 × g for 5 min and the
435 supernatant was decanted. The cell pellet was then resuspended in 6 mL 15% DMEM (no antibiotics)
436 and plated at 1 mL/dish in collagen-coated 35 mm dishes (collagen was neutralized with DMEM medium
437 before cell plating). The feeder cells were incubated in a 37° C incubator overnight. The media was
438 replaced with 2 mL fresh 15% DMEM medium the next day. On the day of $CD34^+$ HSPC cell sort, the
439 media was removed and replaced sorted CB cells in 2.5 mL of LTC media (STEMCELL Technologies
440 #05150) supplemented with 10 µM Hydrocortisone (STEMCELL Technologies #07904).

441 Weekly half-medium changes were performed by removing one half of the medium containing
442 cells and replacing with freshly prepared H5100 with 10 µM hydrocortisone over the 40-day culture
443 period.

444

445 **Colony-forming cell (CFC) assay**

446 For primary CFCs, 500 of sorted lentivirally transduced $CD34^+$ HSPCs were seeded into 1 mL of
447 MethoCultTM H4434 Classic media (STEMCELL Technologies #04434) supplemented with StemSpan™

448 CC100 and antibiotics, and plated in 35mm CFC dishes (STEMCELL Technologies #27150). Cells were
449 incubated for 10 days before colonies were counted.
450 For secondary CFCs, the media containing the cells were collected from the CFC dishes and
451 transferred into 15mL tubes. PBS with 2% FBS was used to rinse the plates and pooled with the collected
452 media. Cells were spun down at 300 x g for 5min, washed with PBS with 2% FBS. After cell counting, the
453 cells were seeded into fresh CFC dishes in fresh MethoCultTM H4434 Classic media supplemented with
454 StemSpan™ CC100 and antibiotics at 50k cells/mL in each plate. Colonies were counted after 10 days.
455
456 **Mouse bone marrow transplants**
457 C57BL/6J-c2J mice were lethally irradiated at 8.1 Gy and reconstituted with 5-fluoro-uracil-
458 treated bone marrow cells obtained from Pep3B mice retrovirally transduced to express indicated
459 constructs via tail vein injections. C56BL/6J-c2J mice were obtained from The Jackson Laboratory. Pep3B
460 mice were bred in-house at the BC Cancer Research Centre.
461
462 **Xenotransplantation**
463 All experimental procedures were done in accordance with protocols approved by the University
464 of British Columbia Animal Care Committee. NRG-3GS mice (NOD.Cg-*Rag1tm1Mom Il2rgtm1Wjl*
465 Tg(CMV-IL3,CSF2,KITLG)1Eav/J)) were bred and maintained in the Animal Resource Centre of the British
466 Columbia Cancer Research Centre under pathogen-free conditions.
467 Female NRG-3GS mice 8-15 weeks of age were sublethally irradiated with 850 cGy (cesium
468 irradiation, medium dose rate) on the day of intrafemoral injection. 100k $CD34^+$ HSPCs harvested from
469 LTC were injected per mouse. For transplant analysis of *ex vivo* cultured cells, bone marrow aspirates
470 were performed every 6 weeks post-transplant and human chimerism was tracked by flow cytometry
471 analysis (using a BD LSR Fortessa analyzer or BD FACSymphony) and analyzed with the following: APC-
472 anti-CD45 2D1(1:50; Invitrogen 17-9459-42), APC/Cy7 anti-CD45 HI30 (1:50; BioLegend 304014), AF700-
473 anti-CD34 (1:50; BD biosciences 561440), PE/Cy7-anti-CD33 (1:100; Thermo fisher 25-0338-42), PE/Cy7-
474 anti-CD15 (1:100; BD biosciences 560827), BV650-anti-CD19 (1:100; BD biosciences 560827), SB600-anti-
475 CD3(1:50; Invitrogen 83-0037-42), DAPI (1 µg/mL final concentration, Sigma-Aldrich D9542).
476 Bone marrow aspirates were performed on the non-injected femur (BM, weeks 6, 20, and 35 weeks
477 post-transplant) or the injected femur (IF, weeks 12 and 27 weeks post-transplant) to determine human

478 cell chimerism. Engraftment is considered long term if detection threshold of >0.01% $CD45^+$ cells is
479 exceeded at 20 weeks.
480 Transplanted mice were sacrificed at predefined, humane clinical morbidity endpoints. At
481 endpoint, human chimerism in bone marrow (cells flushed from femurs, pelvis and tibias), spleen, and
482 liver were tracked by flow cytometry analysis (using a BD LSR Fortessa analyzer or BD FACSymphony)
483 and analyzed with the following: APC-anti-CD45 2D1(1:50; Invitrogen 17-
484 9459-42), APC/Cy7 anti-CD45 HI30 (1:50; BioLegend 304014), AF700-anti-CD34 (1:50; BD biosciences
485 561440), PE -anti-CD33 (1:50; eBioscience 8012-0337-120), PE/Cy7-anti-CD15 (1:100; BD biosciences
486 560827), BV480-anti-CD14 (1:50; BD biosciences 566190), DAPI (1 µg/mL final concentration, Sigma-
487 Aldrich D9542).
488 For secondary transplants, viably frozen bone marrow harvested at primary transplant
489 endpoints were thawed and added drop-wise into 8mL thawing medium (PBS with 10% FBS and 100
490 µg/mL DNAse final concentration). Cells were spun down at 400 x g for 5 min to remove the
491 supernatant. Cells were counted, and the total amount of harvested bone marrow for each EV and KA
492 mice were transplanted into each sublethally irradiated recipient NRG-3GS by tail vein injection. Half of
493 the harvested bone marrow from each donor FKA mouse was transplanted into each FKA recipient
494 mouse. Secondary transplanted mice were monitored, processed, and analyzed following the
495 procedures for primary transplants.
496
497 **Calculating $CD34^+$ cell output for xenotransplants**
498 The number of human $CD34^+$ cells generated per input $CD34^+$ cell after the LTC-IC and
499 xenotransplant process is calculated based on the assumption that the ratio of the (**A**) number of $CD34^+$
500 cells harvested from the LTC to (**B**) the number of $CD34^+$ cells that were injected into the mice (**C**) X = the
501 number of $CD34^+$ cells that would have been harvested at xenotransplant endpoint if the total amount
502 of $CD34^+$ cells harvested from the LTC were injected into the mice to (**D**) the number of $CD34^+$ cells that
503 were actually harvested from at xenotransplant endpoint. Since equal numbers (100k) of total cells
504 harvested from LTC was injected into recipient mice for xenotransplantation, the number of $CD34^+$
505 transplanted varied between conditions.
506 To calculate the number of $CD34^+$ cell generated by the end of the experiment per $CD34^+$ cell
507 inputted into the LTC-IC experiment, we divide "X" by the number of LTC-IC input $CD34^+$ cell, which is
508 the same for each condition.

509 $$\frac{A}{B} = \frac{C}{D}$$

510 $$\frac{\#CD34^{+} \text{ cells at LTC harvest}}{\text{In vivo } CD34^{+} \text{ input cells injected}} = \frac{X}{\text{Average } \#CD34^{+} \text{ cells in BM at endpoint}}$$

511

512 **RNAseq extraction and RNAseq**

513 $CD34^{+}$ HSPCs were cultured for 24 hours in StemSpanTM SFEM supplemented with StemSpan™
514 CC100, 20 ng/mL recombinant hTPO, 750 nM SR1, 35 nM UM171, DNase (100 ug/mL final
515 concentration), and antibiotics after sorting for lentivirally transduced cells as described above before
516 pelleting at 300 x g for 5 min. Cell pellets were resuspended in TRIzolTM reagent (ThermoFisher
517 #15596026). Total RNA was extracted according to manufacturer guidelines. For RNA precipitation, 5 µg
518 glycogen (Roche #10901393001) was added per sample. 40 ng of RNQA per sample was submitted
519 based on quantification by NanoDropTM. Downstream processing, quality control, and RNAseq was
520 performed at Michael Smith laboratories facilities by 1 x Illumina seq with 150bp PET Indexed Lanes.
521 cDNA was labelled using the Biotin Allonamide Triphosphate protocol. Target hybridization was
522 performed at 45°C, for 16-18hr using the FS450_0001 fluidics protocol for washing. Data was acquired
523 using the Affymetrix GeneChip Scanner 3000. CEL files were imported into R and the probe expression
524 values were normalized using the Robust Multichip Average (RMA) method from the 'oligo' (v.1.50.0)
525 package. Probes that were lowly expressed, defined as not having normalized expression values greater
526 than 4 in at least 3 samples, were filtered out. Probes that ambiguously mapped to multiple genes were
527 filtered out.

528

529 **Ki-67 staining**

530 Lentivirally transduced K562 cells were cultured in Iscove Modified Dulbecco Media with 10%
531 FBS and antibiotics for a week after transduction. Cells were fixed and permeabilized with the BD
532 Fixation and Permeabilization kit (#554714) according to manufacturer protocol. Fixed and
533 permeabilized cells were stained with PE anti-human Ki-67 antibody (BioLegend #350504) diluted 1:10 in
534 the BD Perm/Wash buffer from the kit for 30 min on ice. Unbound antibody was washed with the
535 Perm/Wash buffer. Pelleted cells were resuspended in BD Perm/Wash buffer with 2 µg/ml DAPI and
536 incubated for 10 min in the dark, on ice. Cells were centrifuged at 1500 x g for 5 min and resuspended in
537 PBS with 2% FBS and strained for flow cytometry analysis.

538

539 **Histology**

540 Mouse brain samples were fixed in 10% buffered formalin and stored at 4°C for a week before
541 paraffin embedding. H&E and myeloperoxidase staining of brain samples were performed at BC Cancer
542 Vancouver Center Pathology office. Bone marrow smears were stained with Wright-Giemsa staining
543 solution.

544

545 **Immunoprecipitation**

546 For co-immunoprecipitations for identifying protein-protein interactions, cells were washed in
547 PBS then lysed with modified RIPA buffer (50 mM Tris-HCl pH 7.6, 150 mM NaCl, 1 mM EDTA, 1% Triton
548 X-100, protease inhibitor cocktail 1 tablet/1 mL at 1:100 (Sigma-Aldrich 11697498001), phosphatase
549 inhibitor cocktail 1:100 (Sigma-Aldrich P0044-5ML), 1 mM Na3VO4 and 10 mM NaF) for 1 hour at 4°C on
550 a rotating platform, then passed 10x through a 22-G needle. Lysate was centrifuged at 16,000 x g for 10
551 min at 4°C. The supernatant was collected and protein quantification was performed using the BCA
552 assay (BioRad DC Protein assay kit, Bio-Rad 5000112). 1 mg of protein per condition was used for co-
553 immunoprecipitation, and the volume was made up to 1 mL with the lysis buffer. Lysate was precleared
554 with Protein G agarose beads (EMD Millipore 16-266) for FLAG immunoprecipitation or Protein A
555 agarose beads (EMD Millipore 16-125) for LONP1 immunoprecipitation on a rotating platform at 4°C,
556 overnight (16 hours) for FLAG immunoprecipitation or for 3 hours for LONP1 immunoprecipitation.
557 Beads were spun down at 1500 x g for 1 min, and the lysate was transferred to a fresh tube with 50 µL
558 equilibrated ANTI-FLAG® M2 Affinity Gel (Sigma-Aldrich A2220-1ML) for FLAG immunoprecipitation, or
559 with Protein A agarose beads incubated with 2 µg anti-LONP1 antibody (ThermoFisher Scientific 15440-
560 1-AP) overnight (16 hours) and incubated on a rotating platform at 4°C for 1 hour for FLAG
561 immunoprecipitation, and for 3 hours for LONP1 immunoprecipitation. The beads were washed with
562 wash buffer (50 mM Tris-HCl pH 7.6, 150 mM NaCl, 0.05% Triton X-100) 5 times with 1 min 1500 x g
563 spins in between, and eluted in 1x Laemmli sample buffer at 95°C for 15 min.
564 For LONP1 immunoprecipitation to identify post-translational modifications, cells are lysed with RIPA
565 buffer (25mM Tris, 150mM NaCl, 1% NP40, 0.5% sodium deoxycholate, 0.1% sodium dodecyl sulfate
566 (SDS) instead of modified RIPA buffer.

567

568 **Quatitative tandem mass spectrometry**

569 K562 cells lentivirally expressing FLAG-*FBXO11* were lysed in modified RIPA buffer with 10 µM
570 MG132 (ApexBio A2585-25) as described above. Whole cell lysate was incubated with Anti-FLAG® M2
571 Magnetic Beads (Sigma-Aldrich M8823-1ML) or IgG beads for 3 hours then washed with lysis buffer 3
572 times. Three replicates per condition were directly eluted with SP3 elution buffer (200 mM HEPES pH
573 8.0, 10% SDS, 200 mM DTT). Four replicates each were treated with Benzonase® (EMD Millipore 70664-
574 3) before elution. TMT labelling was performed by the mass spectrometry core at the Genome Sciences
575 Centre. 8-plex TMT labels were used. Quantification results were calculated based on published
576 methods[48,49].
577 For the set of immunoprecipitations performed without Benzonase®, proteins had normalized
578 protein enrichment score (PESn) greater than 0.6, and were enriched in 2 of the 3 replicates by at least
579 1.1 fold were shortlisted. For the immunoprecipitations performed with Benzonase® treatment, proteins
580 that had PESn greater than 0.45 and were enriched in 3 of 4 replicates by at least 1.2 fold were
581 shortlisted. The shortlisted proteins from each experiment were intersected to identify commonly
582 immunoprecipitated proteins.
583
584 **Measuring mitochondrial membrane potential**
585 Mitochondrial membrane potential (MMP) was measured by TMRE for cell lines (Cedarlane labs
586 ENZ-52309), or with the JC-1 dye (eBioscience 65-0851-38) for CB.
587 For TMRE, cells were cultured in their regular culture media and conditions with 400 nM TMRE for 30
588 min. Cells were spun down at 400 x g for 5 min to remove the media and TMRE, and the cell pellets were
589 resuspended in PBS with 2% FBS and 1 µg/mL DAPI and kept on ice before analysis by flow cytometry.
590 JC-1 dye was used according to manufacturer protocol. Stained cells were resuspended in PBS with 2%
591 FBS and 1 µg/mL DAPI for flow cytometry analysis.
592
593 **Mitochondrial mass measurements**
594 MitoTracker™ Deep Red FM (FisherScientific M22426) was used to measure mitochondrial mass
595 in K562 cells. Cell staining was performed according to manufacturer protocol. Cells were stained for 30
596 min. Stained cells were washed with PBS with 2% FBS and resuspended in PBS with 2% FBS and 1 µg/mL
597 DAPI for flow cytometry analysis.
598
599 **Ubiquitin, neddylation activating enzyme, and proteasome inhibitor treatment**

600 Ubiquitin activating enzyme (UAE) inhibitors PYR-41 (Sigma-Aldrich N2915-5MG) was used at 50
601 nM, and TAK-243 (also known as MLN7243, Selleck Chemicals S8341) at 0.1 µM. Neddylation activating
602 enzyme (NAE) inhibitors MLN4924 (Cayman Chemical Company 15217) was used at 50 nM, and TAS4464
603 (Selleck Chemicals 15217) was used at 50nM. Proteasome inhibitors MG132 (ApexBio A2585) was used
604 at 1µM, and Bortezomib (Selleck Chemicals S1013) at 50nM. Concentrations were determined by
605 published concentrations used on K562 cells or other myeloid cell lines, and inhibitory effect on global
606 ubiquitination or neddylation levels were confirmed by western blot. Cells were seeded at 300k cells/mL
607 and treated with above inhibitors added directly to culture media for 16 hours. Inhibitor stock solutions
608 were prepared in DMSO.
609
610 **Western blots**
611 Cells were washed with PBS and lysed for 30 min on a rotating platform at 4°C in RIPA buffer
612 (25mM Tris, 150mM NaCl, 1% NP40, 0.5% sodium deoxycholate, 0.1% sodium dodecyl sulfate (SDS),
613 protease inhibitor cocktail, phosphatase inhibitor cocktail, 1 mM Na3VO4 and 10 mM NaF). Lysed cells
614 were centrifuged for 16,000 x g for 10 min at 4°C, and the supernatant was collected for protein
615 quantification by BCA. Samples were mixed with Laemmli sample buffer incubated at 95°C on a heat
616 block for 15 min.
617 Proteins were separated by SDS-polyacrylamide gel electrophoresis at 120 V at room
618 temperature and transferred to nitrocellulose membrane at 100 V at room temperature for 1 hour for
619 proteins of interest under 55 kDa, and at 35 V at 4°C for 16 hours for proteins of interest over 55 kDa.
620 After transfer, blots were rinsed briefly with tris-buffered saline with 0.1% Tween 20 (TBST), and then
621 blocked for 1 hour at room temperature in 5% skim milk in TBST. Membranes were washed 3 times for
622 10 minutes each with TBST.
623 Blots were probed with primary antibodies (FBXO11 antibody at 1:1000, Bethyl Laboratories
624 A301-178A; LONP1 antibody at 1:1000, ThermoFisher Scientific 15440-1-AP; GAPDH antibody at
625 1:10,000, Sigma-Aldrich G8795-200UL, K63 linkage specific antibody at 1:1000, Cell Signaling Technology
626 5621S, NEDD8 antibody at 1:1000, Cell Signaling Technology 2745S; α-tubulin at 1:1000, Sigma-Aldrich
627 T5168-.2ML; TOM20 at 1:1000, New England Biolabs 42406S) prepared in TBST with 1% bovine serum
628 albumin (BSA), based on manufacturer recommended incubation times. Membranes were washed 3
629 times for 10 minutes each with TBST and probed with appropriate HRP secondary antibody (anti-Rabbit
630 Immunoglobulin/HRP, Dako P044801 or aniti-mouse Immunoglobulin/HRP, Dako P0260) at 1:1000 in

631 TBST with 1% BSA. Blots were developed with Western Lightning Plus, Chemiluminescent Substrate
632 (PerkinElmer NEL105) and imaged with a BioRad ChemiDoc MP Imaging system.
633
634 **Seahorse XF Cell MitoStress Test**
635 K562 wild-type control clone and *FBXO11* KO clone cells were in the growth phase at the time of
636 the assay. The cells were counted and seeded at 80k cells per well in the 96-well Agilent Seahorse XF Cell
637 Mito Stress Test (Agilent 103010-100) assay plate. Assay was performed as outlined in the manufacturer
638 protocol and run on the Seahorse XFe bioanalyzer. Analysis and interpretation were done according to
639 protocol.
640
641 **BloodSpot data analysis**
642 Transcriptomic data for SCF genes from the BloodSpot database
643 (https://servers.binf.ku.dk/bloodspot/) were taken from GSE42519 and GSE13159 datasets. Data for
644 *FBXO11* expression taken from the same datasets, with data for the 219208_at probe.
645
646 **RNAseq analysis**
647 RNAseq read alignment was performed using STAR aligner, and count generation was done with
648 Salmon. Variance stabilizing transformation was performed to allow comparison between samples.
649 Transcript per million (TPM) values were filtered to remove genes that have low counts (TPM < 0.5,
650 equivalent to a count of 10 for the dataset) for at least 2 samples. Differential gene expression analysis
651 was performed on the RNAseq data using DeSeq2 package with R. Gene Set Enrichment Analysis was
652 performed using the Hallmark, C2, and C5 gene set collections from MSigDB. GSEA was performed using
653 pre-ranked gene lists for each comparison presented, where the gene list was ranked based on the log2
654 fold change value. CellRadar plots from Figure 4.9 were generated using the public user interface
655 provided by the Karlsson lab (https://karlssong.github.io/cellradar/). The same definition of differentially
656 expressed genes was used, and HSPC data was taken from the BloodSpot HemaExplorer human normal
657 hematopoeisis dataset.
658
659 **Statistical Analysis**
660 Measurements for experiments were taken from distinct samples. All statistical tests were
661 performed using GraphPad Prism version 8.0 (San Diego, California). All data are presented as mean ±

662 standard error of the mean (SEM). Statistical significance was set at a threshold of $P < 0.05$ and FDR <
663 0.25.

664

665 **REFERENCES**

666 1. Döhner, H., Weisdorf, D. J. & Bloomfield, C. D. Acute Myeloid Leukemia. *N Engl J Med* **373**, 1136–
667 1152 (2015).

668 2. Docking, T. R. *et al.* A clinical transcriptome approach to patient stratification and therapy selection
669 in acute myeloid leukemia. *Nat Commun* **12**, 2474 (2021).

670 3. Papaemmanuil, E. *et al.* Genomic Classification and Prognosis in Acute Myeloid Leukemia. *New*
671 *England Journal of Medicine* **374**, 2209–2221 (2016).

672 4. Walker, C. J. *et al.* Gene expression signature predicts relapse in adult patients with cytogenetically
673 normal acute myeloid leukemia. *Blood Advances* **5**, 1474–1482 (2021).

674 5. Baumann, U. *et al.* Disruption of the PRKCD-FBXO25-HAX-1 axis attenuates the apoptotic response
675 and drives lymphomagenesis. *Nat Med* **20**, 1401–1409 (2014).

676 6. Maser, R. S. *et al.* Chromosomally unstable mouse tumours have genomic alterations similar to
677 diverse human cancers. *Nature* **447**, 966–971 (2007).

678 7. Mutations in Fbx4 Inhibit Dimerization of the SCFFbx4 Ligase and Contribute to Cyclin D1
679 Overexpression in Human Cancer - ScienceDirect.
680 https://www.sciencedirect.com/science/article/pii/S1535610808001906.

681 8. Schieber, M. *et al.* FBXO11 is a candidate tumor suppressor in the leukemic transformation of
682 myelodysplastic syndrome. *Blood Cancer J.* **10**, 1–12 (2020).

683 9. Malyukova, A. *et al.* The tumor suppressor gene hCDC4 is frequently mutated in human T-cell acute
684 lymphoblastic leukemia with functional consequences for Notch signaling. *Cancer Res* **67**, 5611–
685 5616 (2007).

686 10. Loh, M. L. *et al.* Mutations in CBL occur frequently in juvenile myelomonocytic leukemia. *Blood* **114**,
687 1859–1863 (2009).

688 11. King, B. *et al.* The ubiquitin ligase FBXW7 modulates leukemia-initiating cell activity by regulating
689 MYC stability. *Cell* **153**, 1552–1566 (2013).
690 12. Reavie, L. *et al.* Regulation of hematopoietic stem cell differentiation by a single ubiquitin ligase–
691 substrate complex. *Nat Immunol* **11**, 207–215 (2010).
692 13. Crusio, K. M., Reavie, L. B. & Aifantis, I. Regulation of hematopoietic stem cell fate by the ubiquitin
693 proteasome system. *Trends Immunol* **33**, 357–363 (2012).
694 14. Abdel-Rahman, M. H. *et al.* Germline BAP1 mutation predisposes to uveal melanoma, lung
695 adenocarcinoma, meningioma, and other cancers. *J Med Genet* **48**, 10.1136/jmedgenet-2011–
696 100156 (2011).
697 15. Meyer, T. *et al.* Functional characterization of BRCC3 mutations in acute myeloid leukemia with
698 t(8;21)(q22;q22.1). *Leukemia* **34**, 404–415 (2020).
699 16. Horton, T. M. *et al.* A Phase 2 Study of Bortezomib Combined with Either Idarubicin/Cytarabine or
700 Cytarabine/Etoposide in Children with Relapsed, Refractory or Secondary Acute Myeloid Leukemia:
701 A Report from the Children's Oncology Group. *Pediatr Blood Cancer* **61**, 1754–1760 (2014).
702 17. Tyner, J. W. *et al.* Functional genomic landscape of acute myeloid leukaemia. *Nature* **562**, 526–531
703 (2018).
704 18. Bottomly, D. *et al.* Integrative analysis of drug response and clinical outcome in acute myeloid
705 leukemia. *Cancer Cell* (2022) doi:10.1016/j.ccell.2022.07.002.
706 19. Genomic and Epigenomic Landscapes of Adult De Novo Acute Myeloid Leukemia. *New England*
707 *Journal of Medicine* **368**, 2059–2074 (2013).
708 20. Bolouri, H. *et al.* The molecular landscape of pediatric acute myeloid leukemia reveals recurrent
709 structural alterations and age-specific mutational interactions. *Nat Med* **24**, 103–112 (2018).
710 21. Lindsley, R. C. *et al.* Acute myeloid leukemia ontogeny is defined by distinct somatic mutations.
711 *Blood* **125**, 1367–1376 (2015).

712 22. Ma, W. *et al.* Ubiquitin-proteasome system profiling in acute leukemias and its clinical relevance.
713 *Leuk Res* **35**, 526–533 (2011).
714 23. Xie, S. Z. *et al.* Sphingolipid Modulation Activates Proteostasis Programs to Govern Human
715 Hematopoietic Stem Cell Self-Renewal. *Cell Stem Cell* **25**, 639-653.e7 (2019).
716 24. Xu, P. *et al.* FBXO11-mediated proteolysis of BAHD1 relieves PRC2-dependent transcriptional
717 repression in erythropoiesis. *Blood* **137**, 155–167 (2021).
718 25. Higuchi, M. *et al.* Expression of a conditional AML1-ETO oncogene bypasses embryonic lethality and
719 establishes a murine model of human t(8;21) acute myeloid leukemia. *Cancer Cell* **1**, 63–74 (2002).
720 26. Yuan, Y. *et al.* AML1-ETO expression is directly involved in the development of acute myeloid
721 leukemia in the presence of additional mutations. *PNAS* **98**, 10398–10403 (2001).
722 27. Chou, F.-S., Wunderlich, M., Griesinger, A. & Mulloy, J. C. N-Ras(G12D) induces features of stepwise
723 transformation in preleukemic human umbilical cord blood cultures expressing the AML1-ETO
724 fusion gene. *Blood* **117**, 2237–2240 (2011).
725 28. Gibellini, L. *et al.* LonP1 Differently Modulates Mitochondrial Function and Bioenergetics of Primary
726 Versus Metastatic Colon Cancer Cells. *Front Oncol* **8**, 254 (2018).
727 29. Maneix, L. *et al.* The Mitochondrial Protease LonP1 Promotes Proteasome Inhibitor Resistance in
728 Multiple Myeloma. *Cancers (Basel)* **13**, 843 (2021).
729 30. Quirós, P. M. *et al.* ATP-Dependent Lon Protease Controls Tumor Bioenergetics by Reprogramming
730 Mitochondrial Activity. *Cell Reports* **8**, 542–556 (2014).
731 31. Ghosh, J. C. *et al.* Akt phosphorylation of mitochondrial Lonp1 protease enables oxidative
732 metabolism and advanced tumor traits. *Oncogene* **38**, 6926–6939 (2019).
733 32. Mansell, E. *et al.* Mitochondrial Potentiation Ameliorates Age-Related Heterogeneity in
734 Hematopoietic Stem Cell Function. *Cell Stem Cell* **28**, 241-256.e6 (2021).

735 33. Romero-Moya, D. *et al.* Cord blood-derived CD34+ hematopoietic cells with low mitochondrial mass
736 are enriched in hematopoietic repopulating stem cell function. *Haematologica* **98**, 1022–1029
737 (2013).
738 34. Vannini, N. *et al.* Specification of haematopoietic stem cell fate via modulation of mitochondrial
739 activity. *Nat Commun* **7**, 13125 (2016).
740 35. Abida, W. M., Nikolaev, A., Zhao, W., Zhang, W. & Gu, W. FBXO11 Promotes the Neddylation of p53
741 and Inhibits Its Transcriptional Activity. *J Biol Chem* **282**, 1797–1804 (2007).
742 36. Liu, M. *et al.* Macrophage K63-Linked Ubiquitination of YAP Promotes Its Nuclear Localization and
743 Exacerbates Atherosclerosis. *Cell Reports* **32**, (2020).
744 37. Duan, S. *et al.* FBXO11 targets BCL6 for degradation and is inactivated in diffuse large B-cell
745 lymphomas. *Nature* **481**, 90–93 (2012).
746 38. Rossi, M. *et al.* Regulation of the CRL4(Cdt2) ubiquitin ligase and cell-cycle exit by the SCF(Fbxo11)
747 ubiquitin ligase. *Mol Cell* **49**, 1159–1166 (2013).
748 39. Jin, Y. *et al.* FBXO11 promotes ubiquitination of the Snail family of transcription factors in cancer
749 progression and epidermal development. *Cancer Letters* **362**, 70–82 (2015).
750 40. Cole, A. *et al.* Inhibition of the Mitochondrial Protease ClpP as a Therapeutic Strategy for Human
751 Acute Myeloid Leukemia. *Cancer Cell* **27**, 864–876 (2015).
752 41. Gibellini, L. *et al.* Chapter One - The biology of Lonp1: More than a mitochondrial protease. in
753 *International Review of Cell and Molecular Biology* (ed. Galluzzi, L.) vol. 354 1–61 (Academic Press,
754 2020).
755 42. Shin, C.-S. *et al.* LONP1 and mtHSP70 cooperate to promote mitochondrial protein folding. *Nat*
756 *Commun* **12**, 265 (2021).
757 43. Choi, C. H., Zimon, A. & Usheva, A. Metabolic stress regulates basic transcription through acetyl-
758 coenzyme A. *CMLS, Cell. Mol. Life Sci.* **62**, 625 (2005).

759 44. Martín-Martín, N., Carracedo, A. & Torrano, V. Metabolism and Transcription in Cancer: Merging
760 Two Classic Tales. *Frontiers in Cell and Developmental Biology* **5**, 119 (2018).
761 45. Sanin, D. E. *et al.* Mitochondrial Membrane Potential Regulates Nuclear Gene Expression in
762 Macrophages Exposed to Prostaglandin E2. *Immunity* **49**, 1021-1033.e6 (2018).
763 46. Cheng, D. T. *et al.* Memorial Sloan Kettering-Integrated Mutation Profiling of Actionable Cancer
764 Targets (MSK-IMPACT). *J Mol Diagn* **17**, 251–264 (2015).
765 47. Jaiswal, S. *et al.* Age-Related Clonal Hematopoiesis Associated with Adverse Outcomes. *New*
766 *England Journal of Medicine* **371**, 2488–2498 (2014).
767 48. Griffin, N. M. *et al.* Label-free, normalized quantification of complex mass spectrometry data for
768 proteomic analysis. *Nat Biotechnol* **28**, 83–89 (2010).
769 49. Lavallée-Adam, M., Rauniyar, N., McClatchy, D. B. & Yates, J. R. PSEA-Quant: A Protein Set
770 Enrichment Analysis on Label-Free and Label-Based Protein Quantification Data. *J. Proteome Res.*
771 **13**, 5496–5509 (2014).
772
773
774
775

a

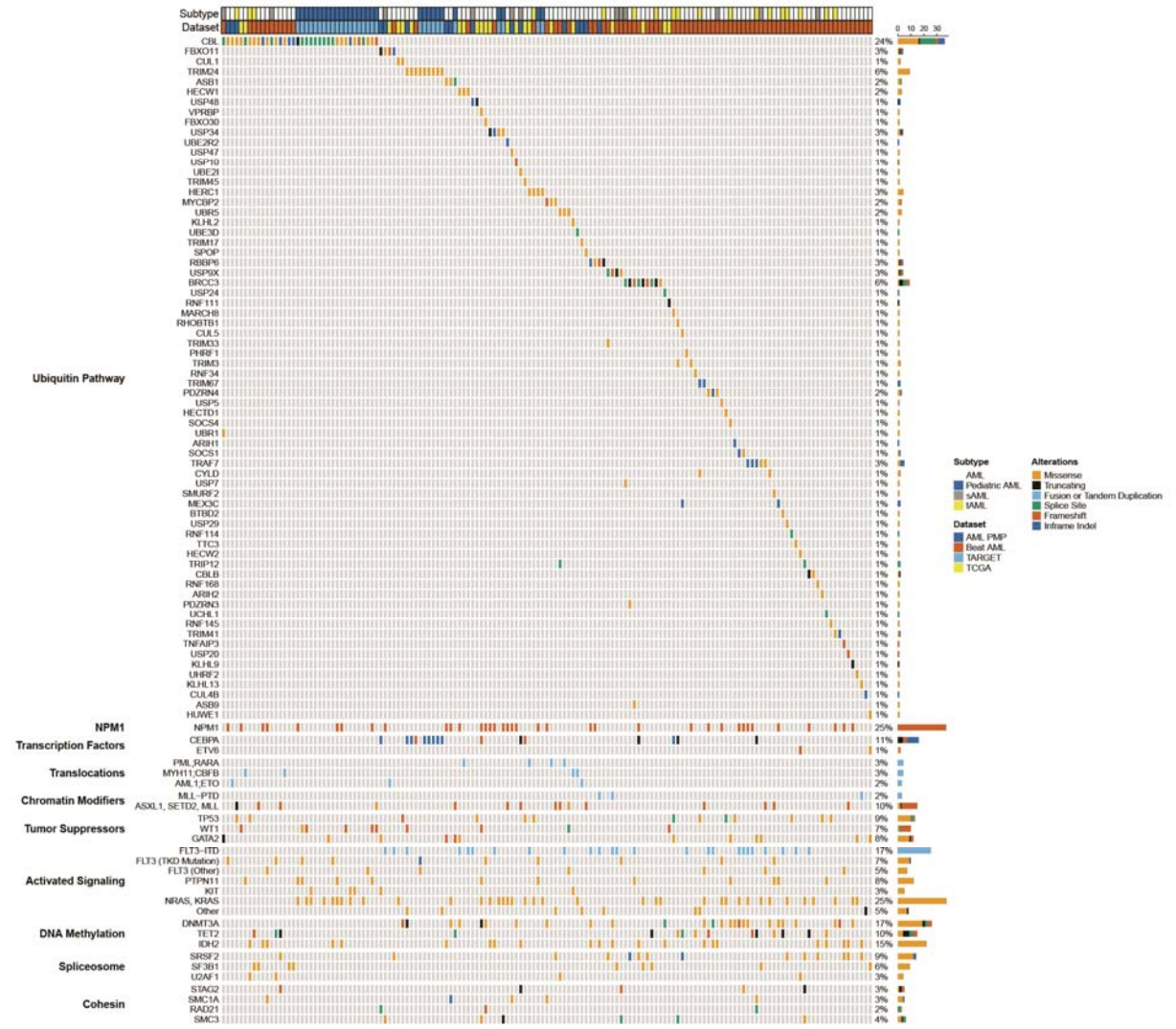
Subtype
Dataset
Ubiquitin Pathway
NPM1
Transcription Factors
Translocations
Chromatin Modifiers
Tumor Suppressors
Activated Signaling
DNA Methylation
Spliceosome
Cohesin
Subtype
AML
Pediatric AML
sAML
tAML
Dataset
AML PMP
Beat AML
TARGET
TCGA
Alterations
Missense
Truncating
Fusion or Tandem Duplication
Splice Site
Frameshift
Inframe Indel

b

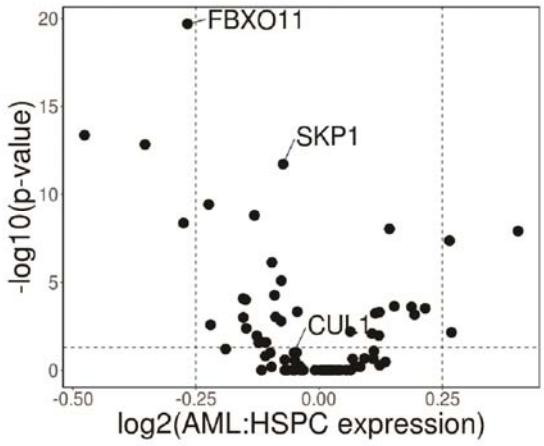
FBXO11
SKP1
CUL1
-log10(p-value)
log2(AML:HSPC expression)

c

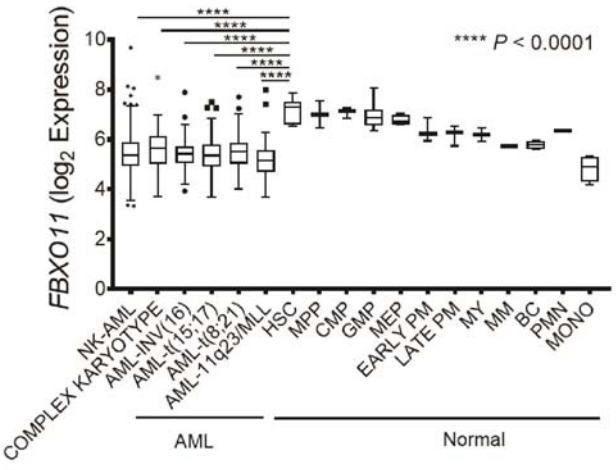
**** P < 0.0001
FBXO11 (log2 Expression)
NK-AML
COMPLEX KARYOTYPE
AML-INV(16)
AML-t(15;17)
AML-t(8;21)
AML-11q23/MLL
HSC
MPP
CMP
GMP
MEP
EARLY PM
LATE PM
MY
MM
BC
PMN
MONO
AML
Normal

777 **Figure 1. Aberration of ubiquitin pathway gene sequence or expression is frequent in AML**
778 **a**, AML patients with ubiquitin pathway mutations from AML PMP, TCGA, TARGET, and Beat AML data
779 sets are represented in an oncoprint. Shown are 149 of 1,727 AML patients with ubiquitin pathway
780 mutations along with co-occurring somatic mutations. Columns represent individual AML samples, and
781 rows represent individual genes. **b**, Shown is a volcano plot comparing transcript expression of SCF
782 genes. Bonferroni-adjusted *P* values represent *t*-tests. The horizontal dotted line represents $P = 0.05$.
783 Vertical lines represent $\log_2$ fold change of $|0.25|$. **c**, Expression levels of *FBXO11* transcripts across
784 different AML subtypes and normal hematopoietic populations from BloodSpot are represented as a box
785 and whisker plot. The median is shown with a horizontal line, with the edges of the box corresponding
786 to the first and third quartiles of the distribution, with whiskers extending to 1.5* the inter-quartile
787 range of the distribution. *P* values represent two-tailed *t*-tests.
788

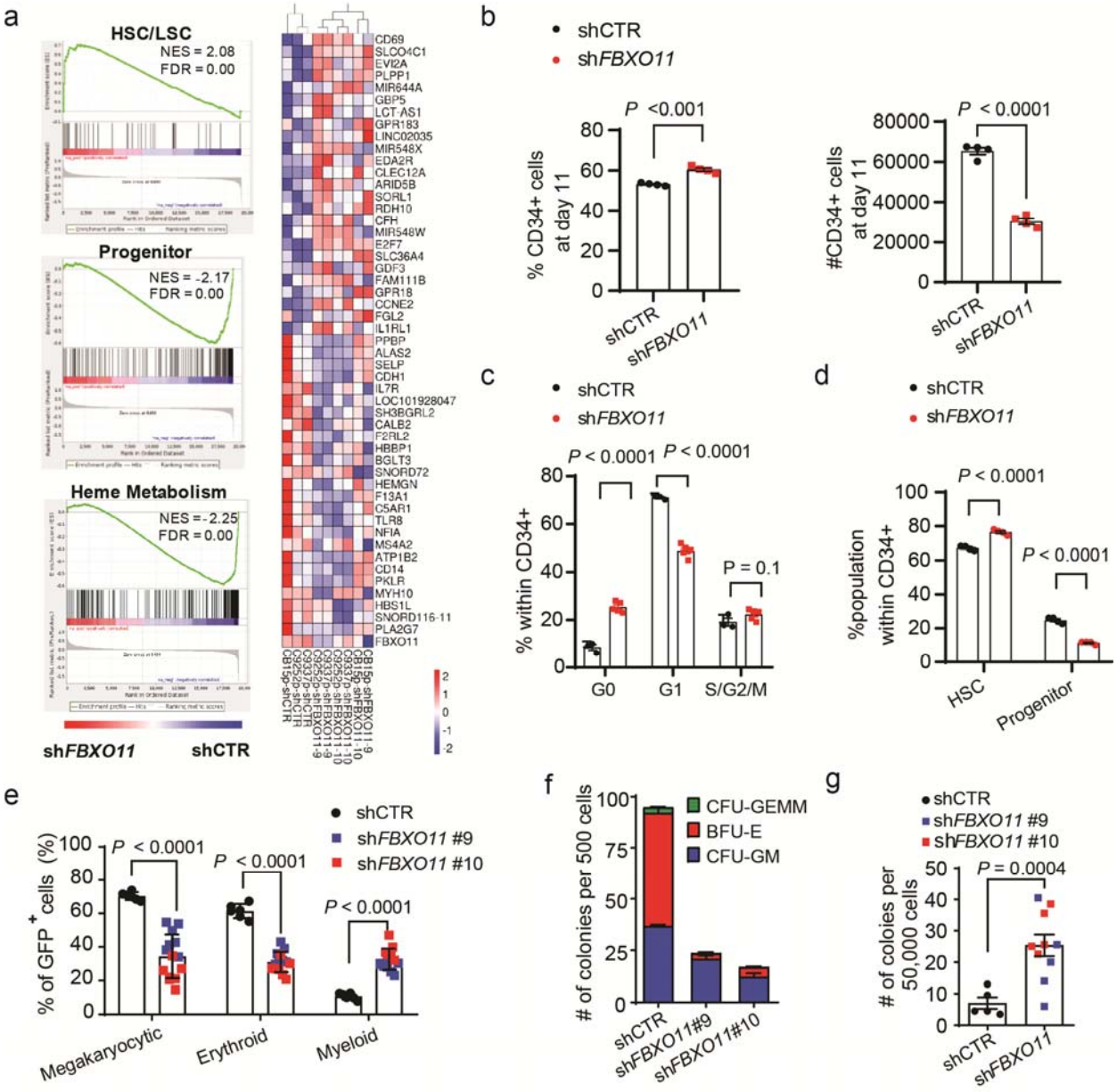

Figure 2. *FBXO11* depletion promotes quiescence and blocks differentiation.

a, Shown are Gene Set Enrichment Analysis plots for the EPPERT_CE_HSC_LSC (HSC/LSC), EPPERT_PROGENITOR (Progenitor), and HALLMARK_HEME_METABOLISM (Heme Metabolism) gene sets comparing CD34$^+$ HSPC with *FBXO11* depletion (sh*FBXO11*) to cells expressing non-targeting control shRNA (shCTR). The heatmap on the right is arranged according to pairwise clustering based on the 25 most upregulated and 25 most downregulated genes in *FBXO11*-depleted cells compared to control. **b**, Shown are percentages and absolute cell counts of CD34$^+$ HSPC expressing shCTR or sh*FBXO11* at day 7 of culture (n = 4 independent replicates). **c**, Cell cycle state of CD34$^+$ HSPC was measured by Ki-67/DAPI staining (n = 3 (shCTR), n = 5 (sh*FBXO11*) independent replicates). **d**, Percentages of CD45RA$^-$ (corresponding to cultured HSC immunophenotype) and CD45RA$^+$90$^-$ (corresponding to cultured hematopoietic progenitor (HPC) immunophenotype) cells within the CD34$^+$ population are shown (n = 4

801 (shCTR), *n* = 4 (sh*FBXO11*) independent replicates). **e**, Shown are percentages of megakaryocytic ($CD41^+$
802 $CD61^+$), erythroid ($CD71^+$ Glycophorin A/B^+), and myeloid ($CD15^+$) cells in $CD34^+$ HSPC expressing shCTR
803 or sh*FBXO11* after 7 days of culture. **f**, Primary CFC from $CD34^+$ HSPC expressing shCTR or sh*FBXO11*
804 were counted 12 days after plating (*n* = 5 independent replicates). **g**, Colony counts following secondary
805 plating of 50,000 cells from the primary CFC assay shown in panel (f) (*n* = 5 independent replicates). *P*
806 values represent two-tailed *t*-test, and error bars represent s.d.

807

808

809

810

811

812

813

814

815

816

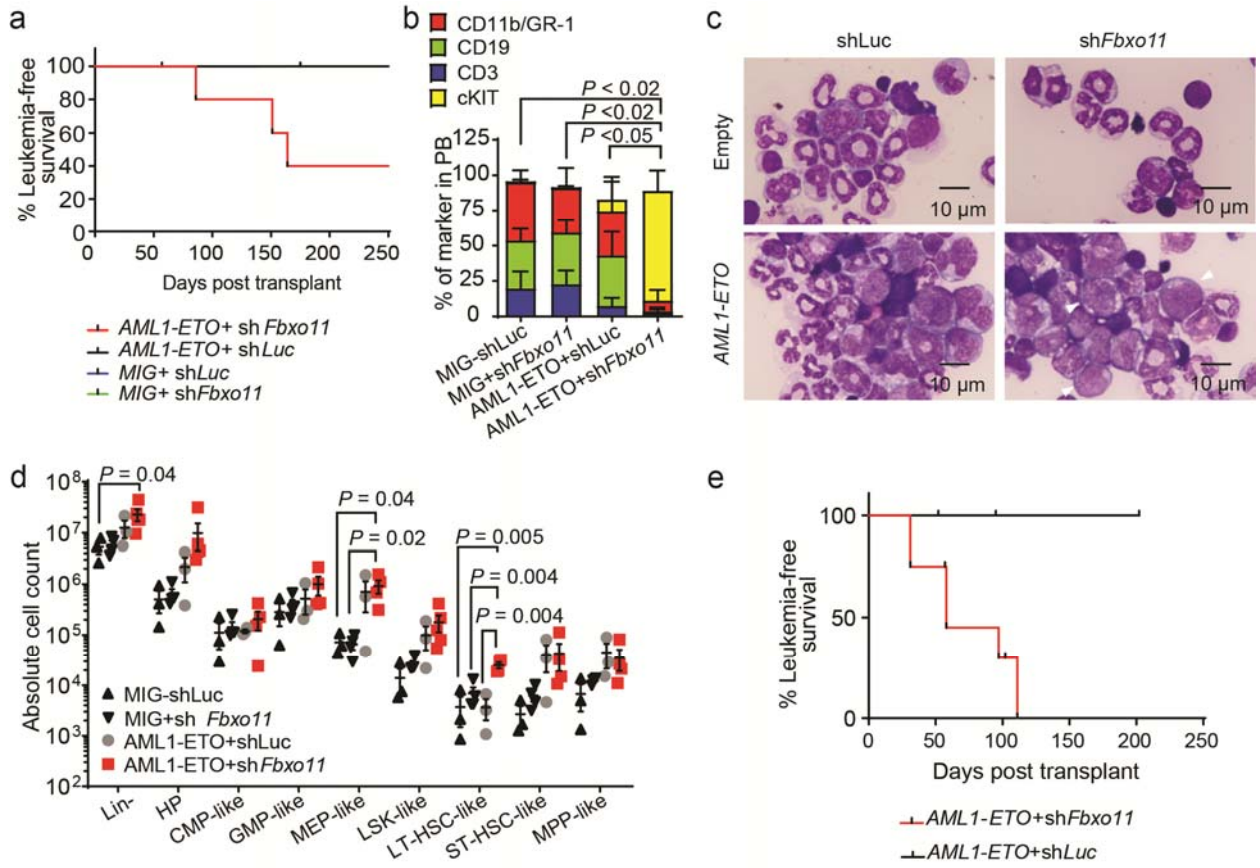

Figure 3. *Fbxo11* depletion cooperates with *AML1-ETO* to generate AML in mice.
a, The Kaplan-Meier plot shows survival data for mice transplanted with HSPC expressing *AML1-ETO* fusion cDNA or empty vector (MIG) and retrovirus expressing an shRNA against murine *Fbxo11* (sh*Fbxo11*) or control shRNA against luciferase (shLuc) (n = 4-5 mice). P = 0.06 for *AML1-ETO* + sh*Fbxo11*vs *AML1-ETO* + sh*Luc* (Mantel-Cox test). **b**, Peripheral blood cell expression of myeloid (CD11/GR-1), B-cell (CD19), T-cell (CD3), and myeloid progenitor (lineage-negative, c-KIT positive) surface markers were measured at endpoint by flow cytometry. **c**, Giemsa-stained bone marrow cytospins from representative animals from panel (a) at endpoint. Arrows point to blast cells. **d**, Absolute cell counts of bone marrow cells expressing cell surface markers corresponding to normal HSPC populations were determined by flow cytometry. Flow cytometry data and gating strategies are shown in Supplementary Figure 6. P values represent two-tailed t-tests, and error bars represent s.d. **e**, Shown are Kaplan-Meier curves following secondary bone marrow transplantation of marrow from 2-4 different primary transplanted animals from panel (a) (n = 4-8 mice); P = 0.07 (Mantel-Cox test)).

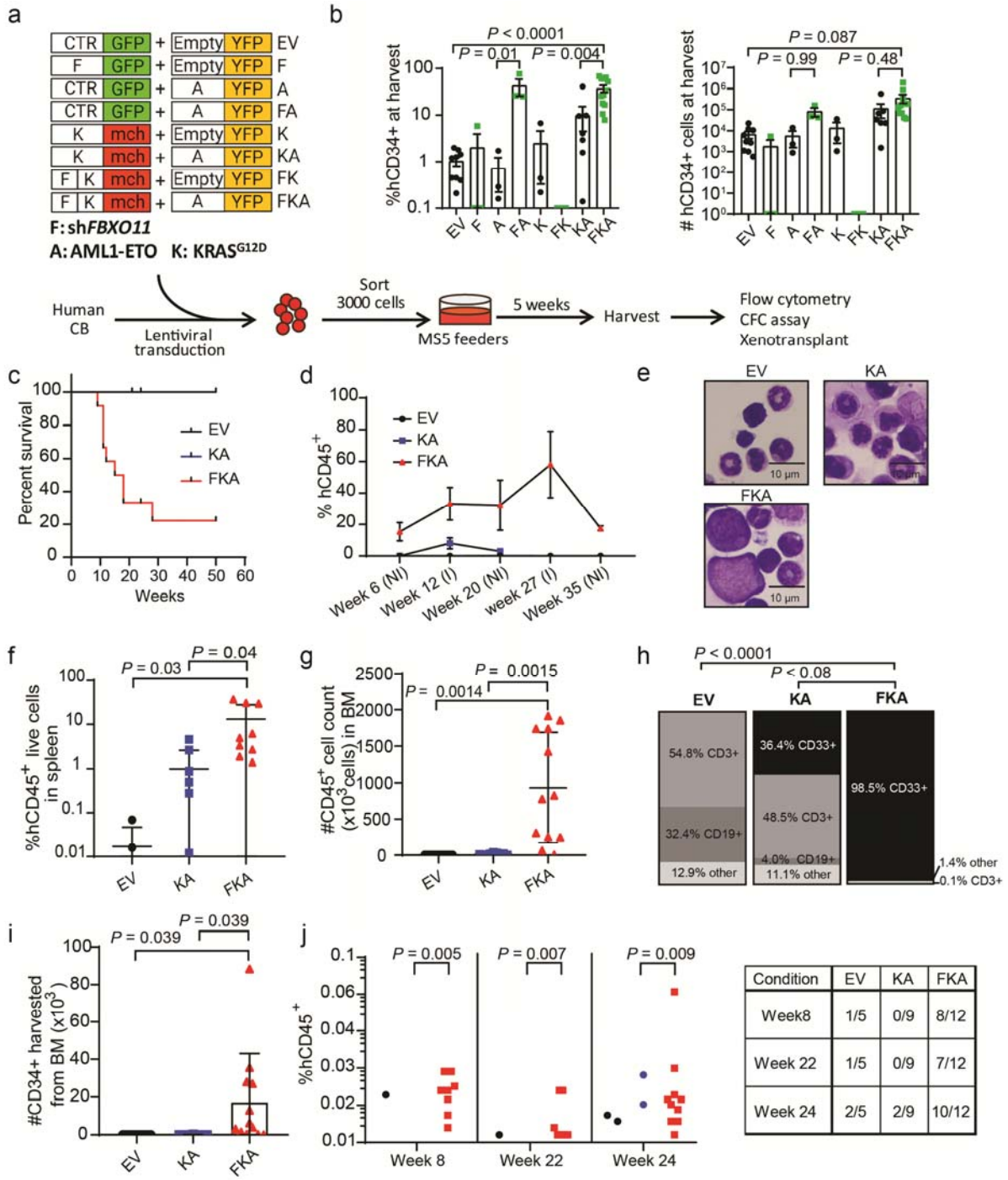

Condition	EV	KA	FKA
Week8	1/5	0/9	8/12
Week 22	1/5	0/9	7/12
Week 24	2/5	2/9	10/12

Figure 4. *FBXO11* depletion cooperates with *AML1-ETO* and *KRAS*^{G12D} to generate human myeloid leukemia.

a, Schematic outlining the experimental design for long-term culture and xenotransplant of CD34$^+$ HSPC. **b**, *FBXO11* knockdown maintains CD34$^+$ cells in long-term culture. Percentages (left panel) and total live cell counts (right panel) of CD34$^+$ cells were measured on day 40 of culture (n = 9 (EV), n = 3 (F, A, FA, K, FK), n = 7 (KA), n = 12 (FKA) independent replicates). **c**, Kaplan-Meier curve for mice transplanted with

838 cells harvested in (b) (P = 0.0028 for EV vs FKA, and P = 0.0002 for KA vs FKA (Mantel-Cox test)). **d**, Bone
839 marrow engraftment of transduced $CD34^+$ cells harvested in (b) (EV, empty vector + control shRNA (n =
840 13); KA, *KRAS*^{G12D} + *AML1-ETO* (n = 9); and FKA, sh*FBXO11* + *KRAS*^{G12D} + *AML1-ETO* (n = 12) mice)
841 showing $CD45^+$ cell chimerism levels in the non-injected bone (NI) or injected bone (I) (P = 0.0033 for EV
842 vs FKA, P = 0.018 for KA vs FKA (Sidak's multiple comparisons test)). **e**, Giemsa-stained bone marrow
843 smear from mice at endpoint. **f**, Human $CD45^+$ hematopoietic cell engraftment in the spleen at endpoint
844 as percentage of total viable spleen cells (n = 5 (EV, 3 not detected (ND)), n = 9 (KA, 1 ND), n = 9 (FKA)
845 mice). **g**, Human $CD45^+$ hematopoietic cell engraftment in the bone marrow measured at endpoint. (n =
846 13 (EV, 7 ND), n = 9 (KA), n = 12 (FKA) mice). **h**, Percentage of lymphoid ($CD3^+$, $CD19^+$), myeloid ($CD33^+$),
847 and other ($CD3^-$ $CD19^-$ $CD33^-$) cells within the viable human $CD45^+$ cell population was measured in bone
848 marrow cells at endpoint. (n = 5 (EV), n = 5 (KA), n = 5 (FKA) mice). **i**, Total $CD34^+$ HSPC numbers in the
849 bone marrow were quantified at endpoint. (n = 13 (EV, 13 ND), n = 9 (KA, 8 ND), n = 12 (FKA) mice). **j**,
850 Hematopoietic cell engraftment in secondary transplants was assessed at weeks 8, 22 and 24. The table
851 on the right lists the fraction of mice in each condition with detectable engraftment at each time point
852 (P values represent Fisher's exact tests). All P values represent two-tailed t-tests unless otherwise
853 specified, and error bars represent s.d.

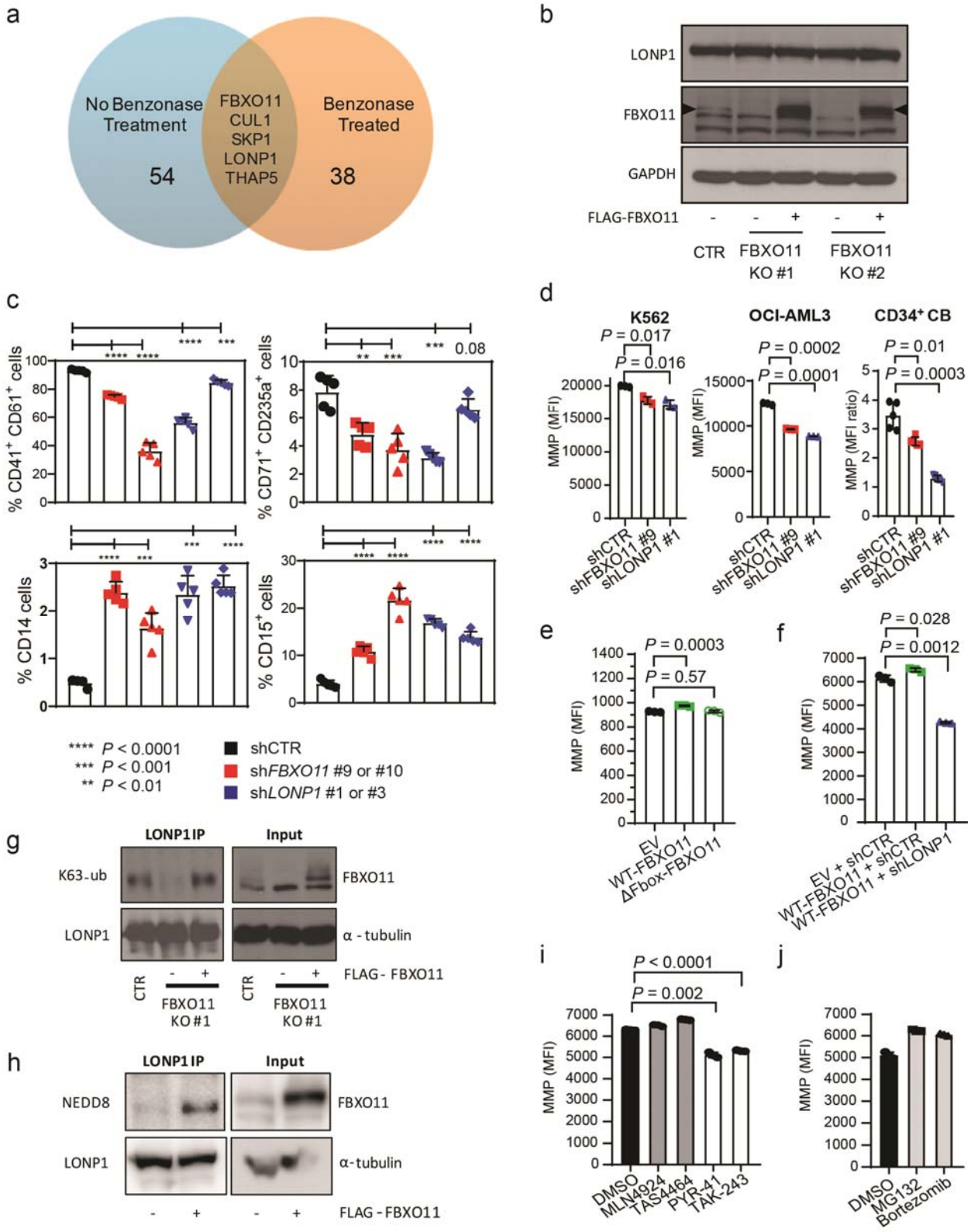

Figure 5. FBXO11 regulates mitochondrial function through activation of LONP1.

856 **a**, Proteins coimmunoprecipitated with FLAG-FBXO11 in K562 cells with or without Benzonase®
857 treatment (*n* = 3 to 4 independent replicates). **b**, Whole cell lysates from K562 parental cells (CTR) or
858 *FBXO11* KO CRISPR clones expressing empty vector or FLAG-tagged FBXO11 (FLAG-FBXO11) were
859 immunoblotted as indicated. **c**, Viable $CD34^+$ HSPC expressing control shRNA (shCTR), sh*FBXO11* or
860 sh*LONP1* were assessed for megakaryocyte ($CD41^+CD61^+$), erythroid ($CD71^+CD235a^+$) or myeloid ($CD14^+$
861 or $CD15^+$) cell surface markers after 7 days of culture (*n* = 4-5 independent replicates). **d**, MMP
862 measured in K562 and OCI-AML3 cells and $CD34^+$ HSPC expressing shRNA targeting *FBXO11* or *LONP1* (*n*
863 = 3 independent replicates). **e**, MMP measured in K562 cells expressing WT *FBXO11* or *FBXO11* with
864 deleted F-box domain (ΔFbox-FBXO11) (*n* = 3 independent replicates). **f**, MMP measured in K562 cells
865 expressing EV with control shRNA (shCTR), or WT-FBXO11 co-expressed with shCTR or shRNA targeting
866 *LONP1* (shLONP1). **g**, Immunoblots of K63-linked polyubiquitination or **h**, neddylation (NEDD8) of LONP1
867 immunoprecipitated from parental K562 cells (CTR) or an *FBXO11* CRISPR KO clone expressing empty
868 vector or FLAG-FBXO11. **i**, MMP measured in K562 cells expressing WT-FBXO11 treated with vehicle
869 (DMSO), neddylation activating enzyme inhibitors (MLN4924 or TAS4464), ubiquitin activating enzyme
870 inhibitors (PYR-41 or TAK-243), or **j,** proteasome inhibitors (MG132 or Bortezomib) (*n* = 3 independent
871 replicates). *P* values represent two-tailed *t*-tests. Error bars represent s.d.

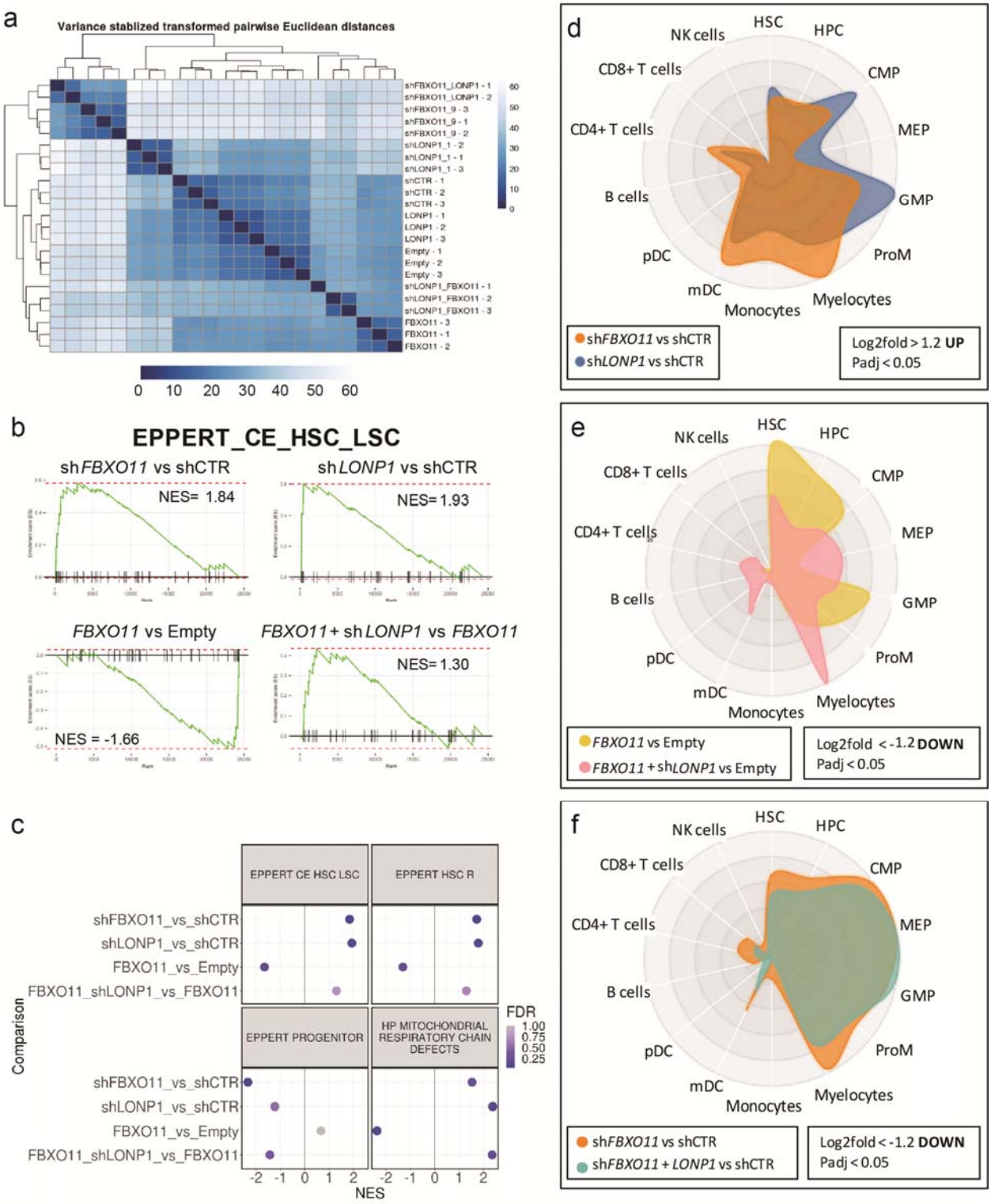

872

873 **Figure 6. *LONP1* is required for functional effects of *FBXO11*.**

874 RNA-seq data from CD34$^+$ HSPC expressing shCTR, sh*FBXO11*, sh*LONP1*, empty vector (Empty or EV),

875 FBXO11, LONP1, FBXO11 with sh*LONP1*, or LONP1 with sh*FBXO11* (*n* = 3 independent replicates except

876 for LONP1 + sh*FBXO11* (*n* = 2 independent replicates)). **a**, Heatmap represents pair-wise Euclidian
877 distances between samples based on expression of all detected genes. **b**, GSEA enrichment plots for the
878 EPPERT_CE_HSC_LSC gene set is shown for various comparisons as noted. **c**, Enrichment trends of
879 various GSEA genesets are summarized for the comparisons listed. Normalized enrichment scores (NES)
880 for each condition are plotted. The false discovery rate (FDR) is represented by the color scale. **d-f**, Cell
881 radar plots were generated using human normal hematopoiesis (HemaExplorer) data from the
882 Bloodspot database. The enrichment of genes associated with different hematopoietic populations
883 indicated are compared between different groups as listed. The closer the outline is to the edge of the
884 plot at a labelled point, the greater the proportion of differentially expressed genes associated with the
885 corresponding cell population. Thresholds for differential gene expression were set at $\log_2$fold > |1.2|
886 and adjusted $P < 0.05$. **d**, Shown are proportions of genes associated with various hematopoietic
887 populations upregulated with *FBXO11* or *LONP1* knockdown compared to control shRNA. **e**, Shown are
888 proportions of genes associated with various hematopoietic populations downregulated with WT
889 *FBXO11* expression, or with *FBXO11* expression combined with *LONP1* knockdown, relative to empty
890 vector control. **f**, Shown are proportions of genes associated with various hematopoietic populations
891 down regulated with *FBXO11* knockdown, or with *FBXO11* knockdown combined with *LONP1*
892 expression, relative to control shRNA.

893

894

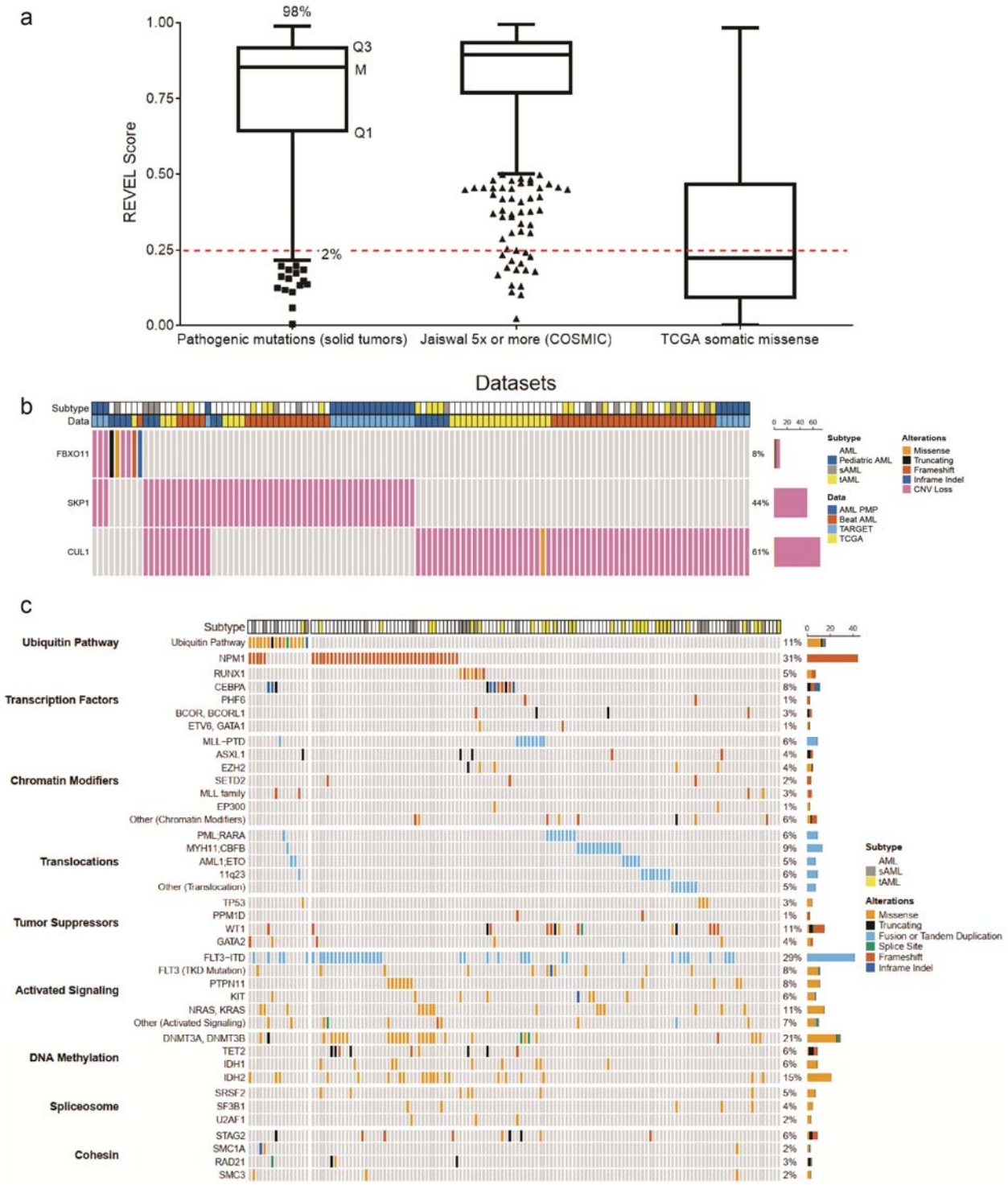

Supplementary Figure 1. Mutations affecting the ubiquitin pathway occur frequently in AML. **a**, REVEL scores for different mutation datasets were compared to identify a threshold for pathogenicity prediction. Mutations plotted include: (1) Known actionable pathogenic missense variants in solid tumors (*n* = 146 variants). (2) Pathogenic variants associated with human hematological cancers

900 (Jaiswal)[1] (*n* = 149 variants). (3) Somatic missense mutations in AML identified in TCGA[2] (*n* = 1233
901 mutations). Applying a minimal REVEL threshold of 0.250, represented by the red dotted horizontal line,
902 removes more than half of all identified somatic missense TCGA variants, while retaining 98% of known
903 pathogenic variants. **b**, Variants affecting the SCF^{FBXO11} complex are summarized in the oncoprint. In the
904 combined AML PMP, TCGA, Beat AML and TARGET pediatric AML datasets, 116 of 1727 AML patients
905 had a mutation or copy loss of a gene affecting the SCF^{FBXO11} complex. **c**, Somatic mutations that satisfy
906 REVEL scores > 0.250 and CADD scores > 10.5 in AML PMP and TCGA AML samples are summarized in
907 the oncoprint. Patients with one or more mutations affecting genes belonging to the ubiquitin pathway
908 are grouped together to the left. AML: *de novo* AML, sAML: transformed AML derived from
909 myelodysplastic syndrome (MDS), tAML: therapy-related AML.

910

911

912

913

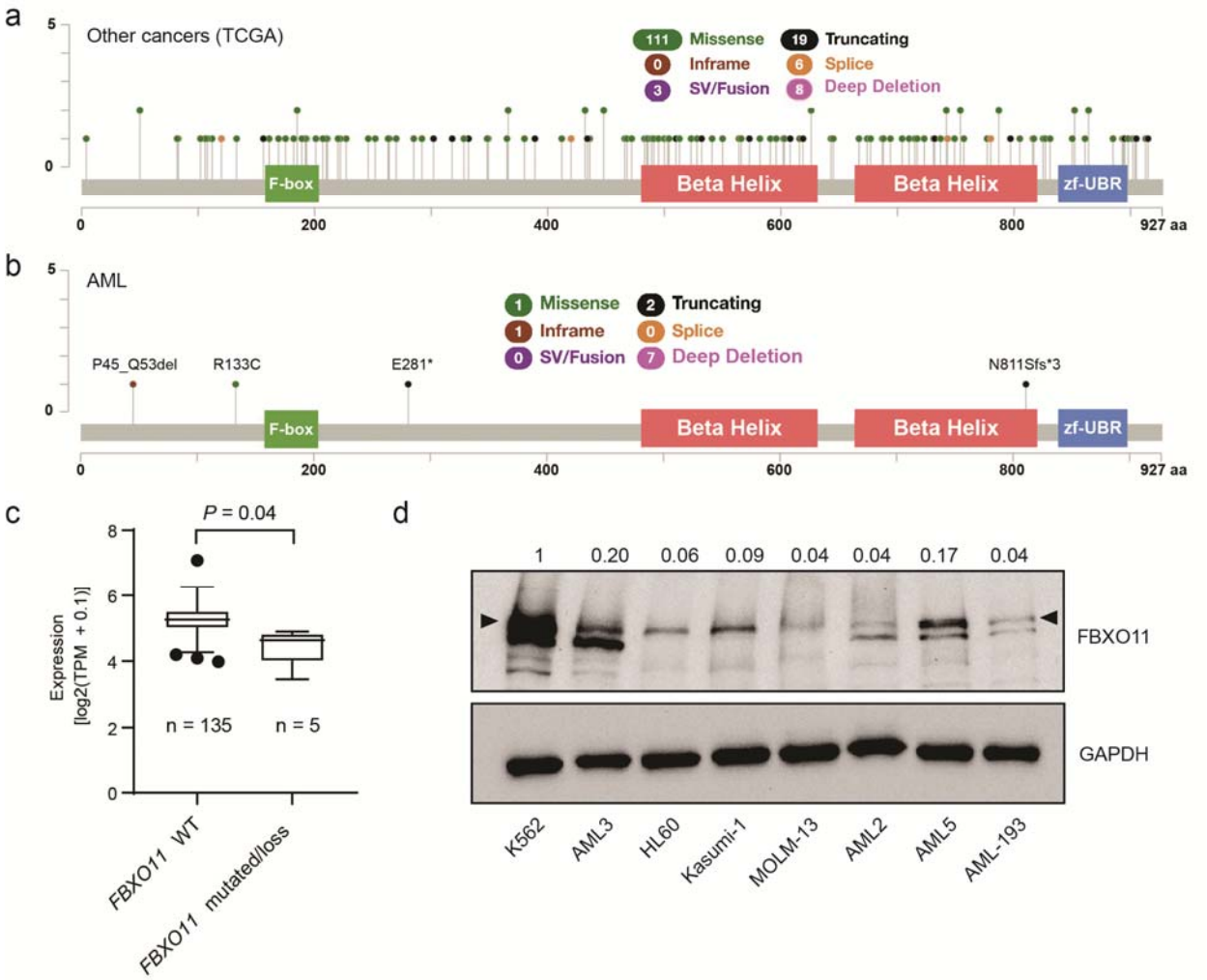

Supplementary Figure 2. *FBXO11* is recurrently mutated in multiple cancers.
a, *FBXO11* mutation types, locations, and frequencies identified in all TCGA cancer samples (n = 10,753) excluding AML samples are shown (cBioPortal). **b**, *FBXO11* mutation types, locations, and frequencies identified in TCGA, Beat AML, TARGET pediatric AML, and AML PMP samples. **c**, *FBXO11* transcript expression in AML PMP samples with mutated/deleted (*FBXO11* mutated/loss) *FBXO11* or WT *FBXO11* represented as a box and whisker plot. **d**, Various myeloid cell lines were immunoblotted for FBXO11 expression. *P* values represent two-tailed *t*-tests and error bars represent s.d.

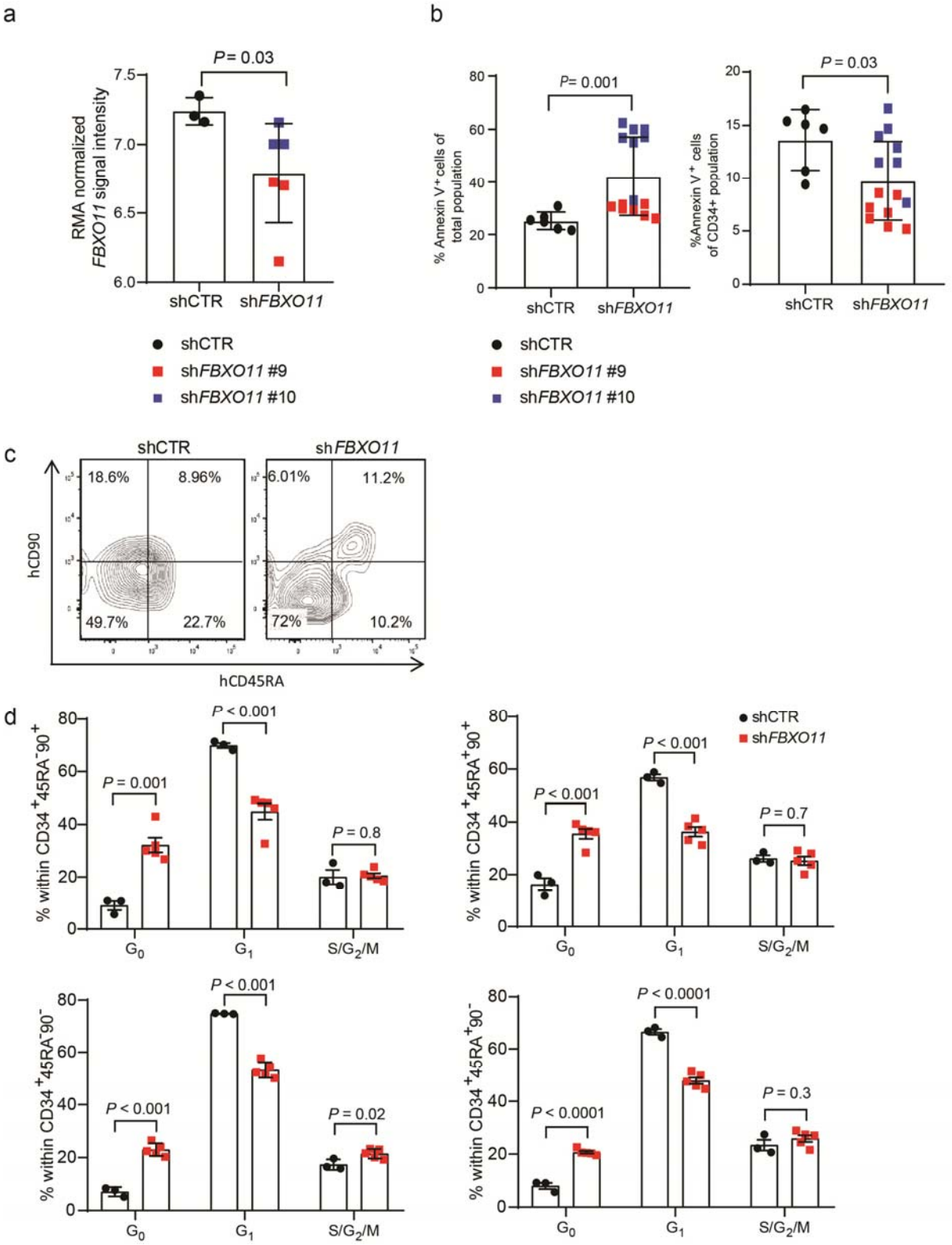

Supplementary Figure 3. CD34⁺ HSPC with *FBXO11* depletion have reduced cell death.

924 **a**, Robust multiarray averaging (RMA) normalized *FBXO11* signal intensity in $CD34^+$ HSPC samples (*n* = 3
925 independent replicates). **b**, The Annexin V^+ population within total (left) or $CD34^+$ (right) cells was
926 analyzed by flow cytometry (*n* = 6 (shCTR), *n* = 7 (sh*FBXO11*) independent replicates). **c**, Representative
927 plot of cultured $CD34^+$ HSPC analyzed for expression of long-term and short-term HSC ($CD90^{+/-}CD45RA^-$)
928 or progenitor ($CD90^-CD45RA^-$) markers. *P* values represent two-tailed *t*-tests and error bars represent
929 s.d. **d**, Cell cycle states of the HSPC populations were determined by Ki-67 staining (*n* = 3 (shCTR), *n* = 5
930 (sh*FBXO11*) independent replicates).

931

932

933

934

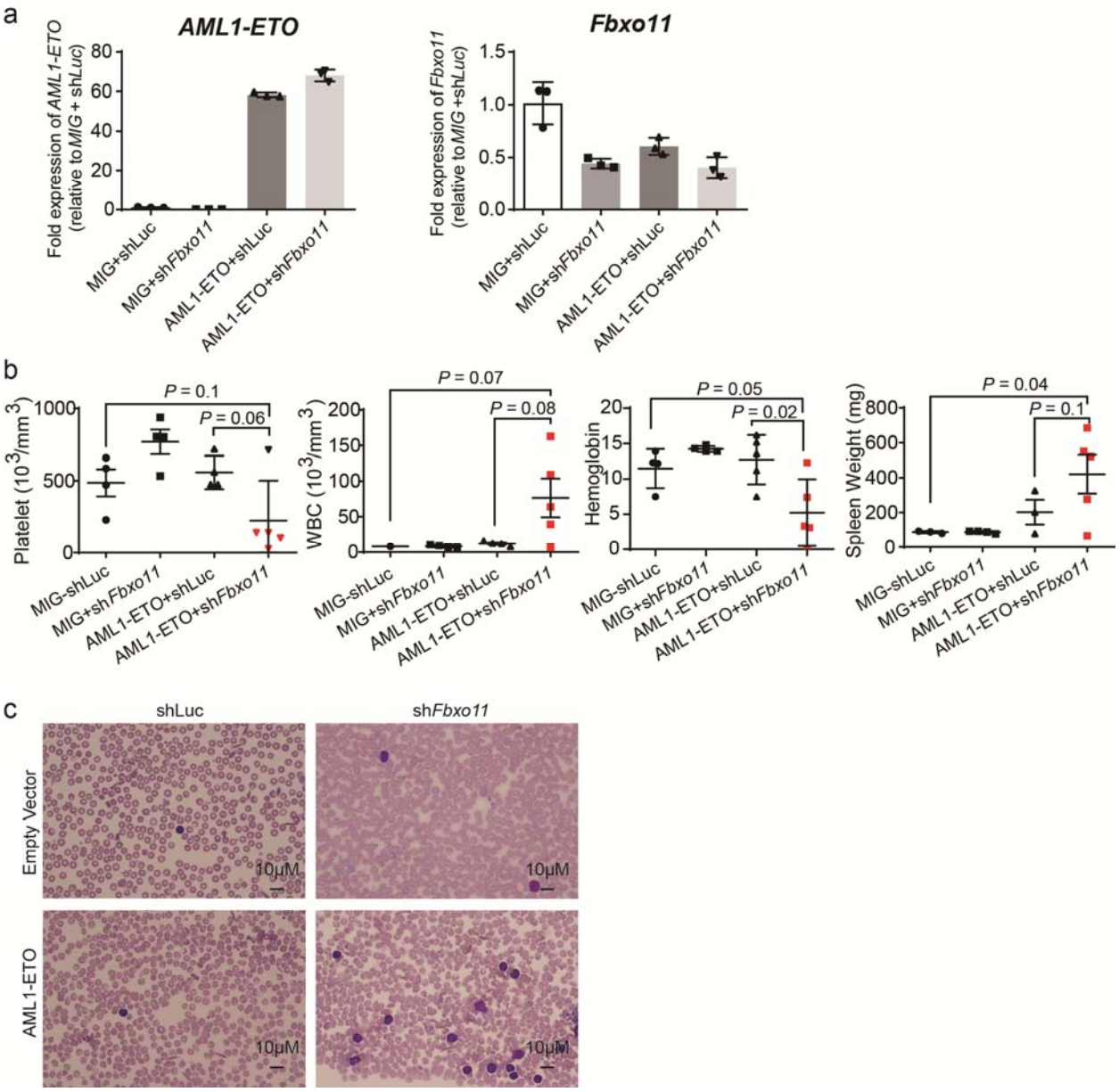

Supplementary Figure 4. *Fbxo11* depletion cooperates with *AML1-ETO* expression to promote leukemogenesis.

a, *AML1-ETO* overexpression and *Fbxo11* knockdown in transduced bone marrow cells were confirmed by RT-qPCR. **b**, Peripheral blood counts and spleen weights were measured at endpoint (n = 3-5, except for n = 1 for MIG-shLuc WBC. P values represent two-tailed t-tests and error bars represent s.d.). **c**, Giemsa stains were performed on peripheral blood smears prepared at endpoint.

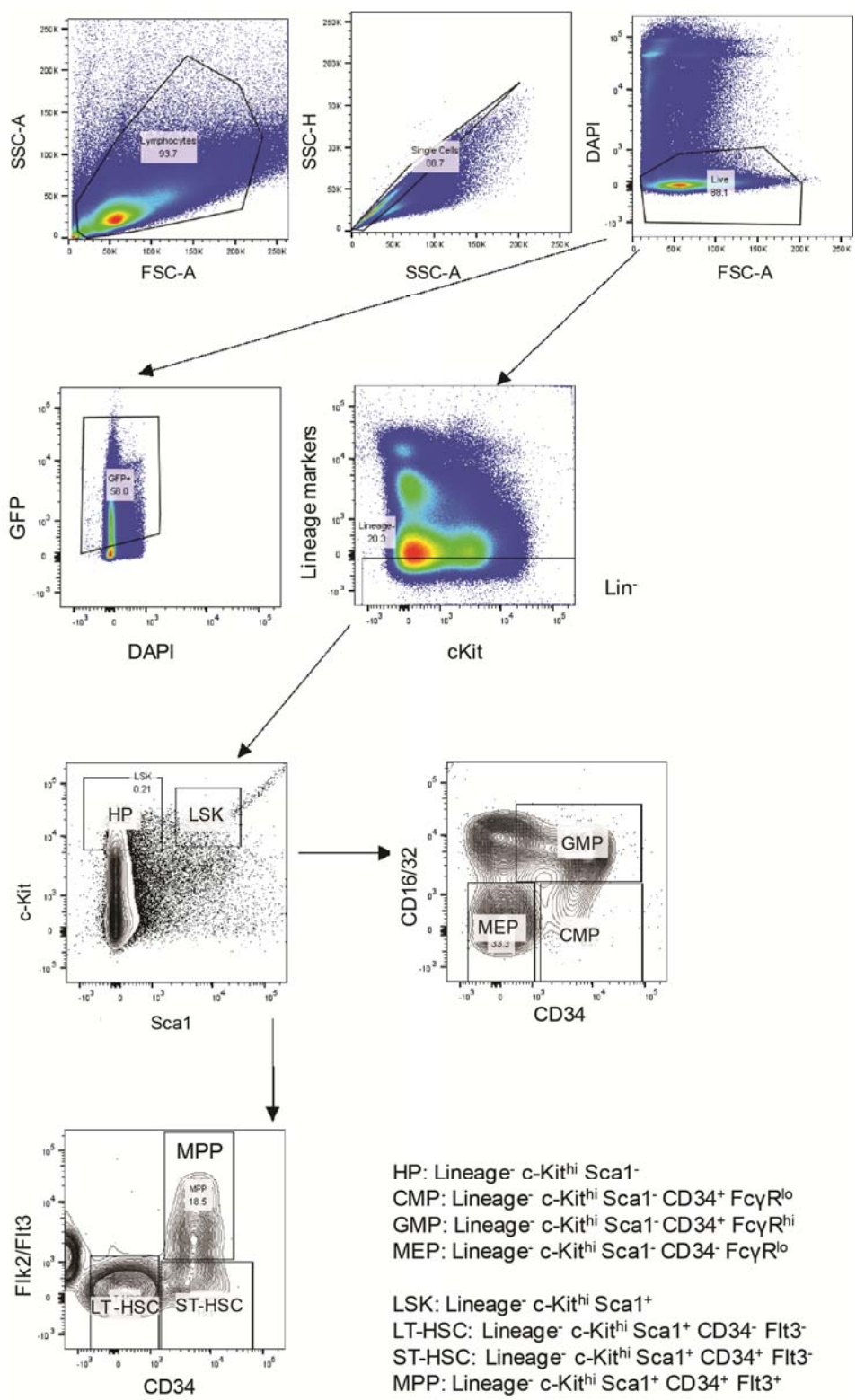

Supplementary Figure 5. Gating strategy for bone marrow flow cytometry analysis at end point.

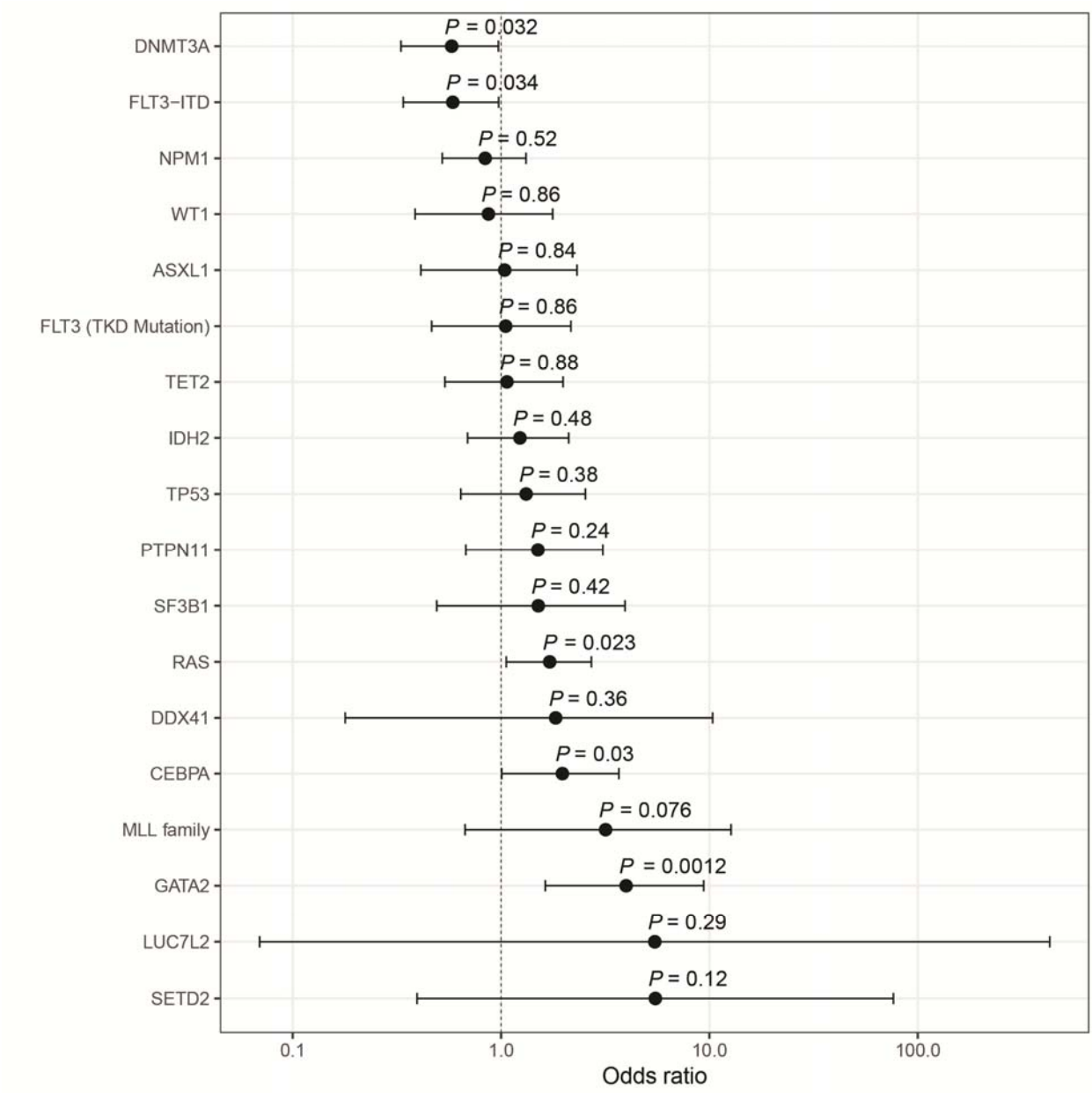

Supplementary Figure 6. Ubiquitin pathway mutations cooccur with *RAS, GATA2,* and *CEBPA* mutations.

Shown are odds ratios of AML-associated mutations for AML PMP samples occurring in ubiquitin pathway-mutated samples compared to samples that are wild-type for ubiquitin pathway genes. Mutations with odds ratio > 1 are likely to co-occur with ubiquitin pathway mutations, and odds ratios < 1 are likely to occur mutually exclusively with ubiquitin pathway mutations. *P* values determined by Fisher's exact test. Bars represent 95% confidence intervals.

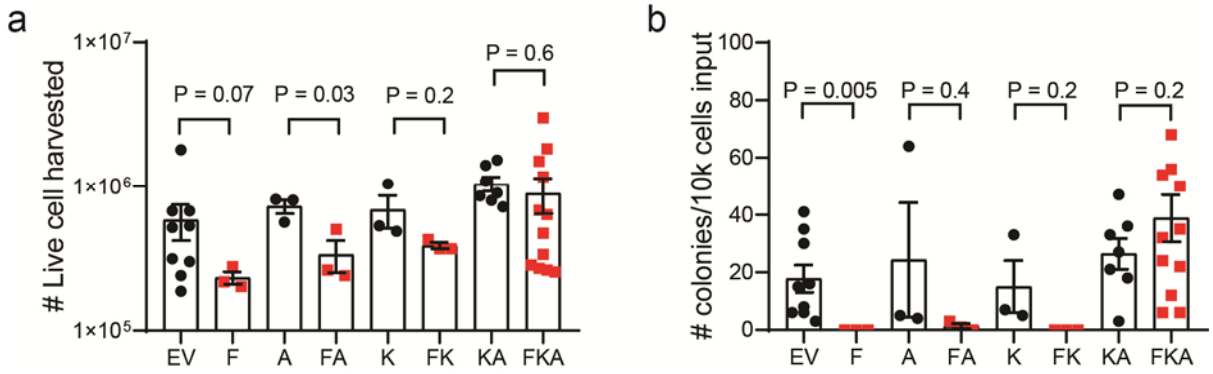

Supplementary Figure 7. Quantification of total cell numbers and CFCs in sh*FBXO11*-, *AML1-ETO*- and *KRAS*^{G12D}- transduced CD34^{+} HSPC harvested after long term culture.

a, Total live cells harvested from long-term culture were counted using trypan blue staining. **b**, CFCs were counted on day 17 after plating (*n* = 3-12 independent replicates). *P* values represent two-tailed *t*-tests and error bars represent s.d. EV = Empty vector and control shRNA; F = sh*FBXO11;* A = *AML1-ETO*; K = *KRAS*^{G12D}; FA = F + A; KA = K + A; FKA = F + K + A.

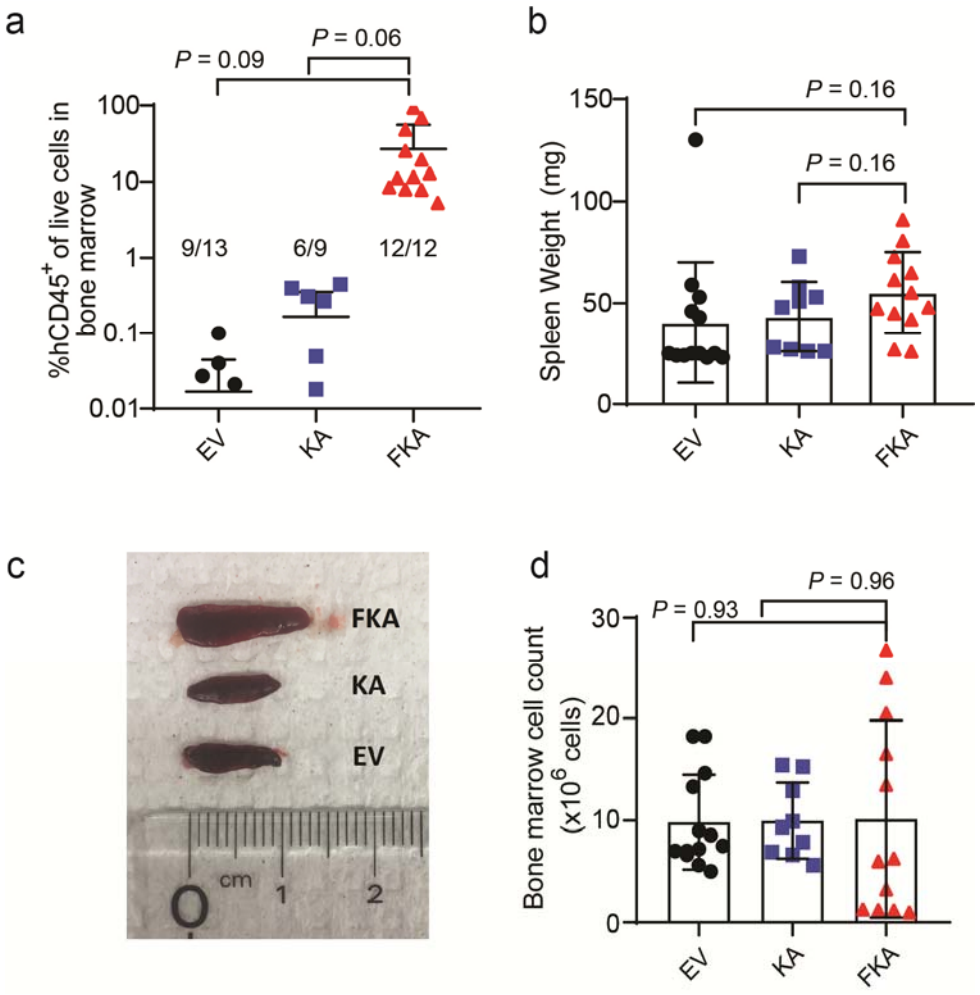

960

961 **Supplementary Figure 8. Analysis of bone marrow and spleen cells from primary xenotransplanted**
962 **mice at endpoint.**
963 **a**, Percentages of CD34$^+$HSPC within the engrafted human hematopoietic cell population at endpoint (*n*
964 = 5-12 mice, ND = not detected for values < 0.01%, *P* values represent Fisher's exact test). **b**, Spleen
965 weights were measured at endpoint (*n* = 9-13 mice). **c**, Representative spleen sizes are shown. **d**, Total
966 live cells harvested from bone marrow at endpoint were counted (*n* = 9-13 mice). *P* values represent
967 two-tailed *t*-tests unless otherwise specified. Error bars represent s.d..

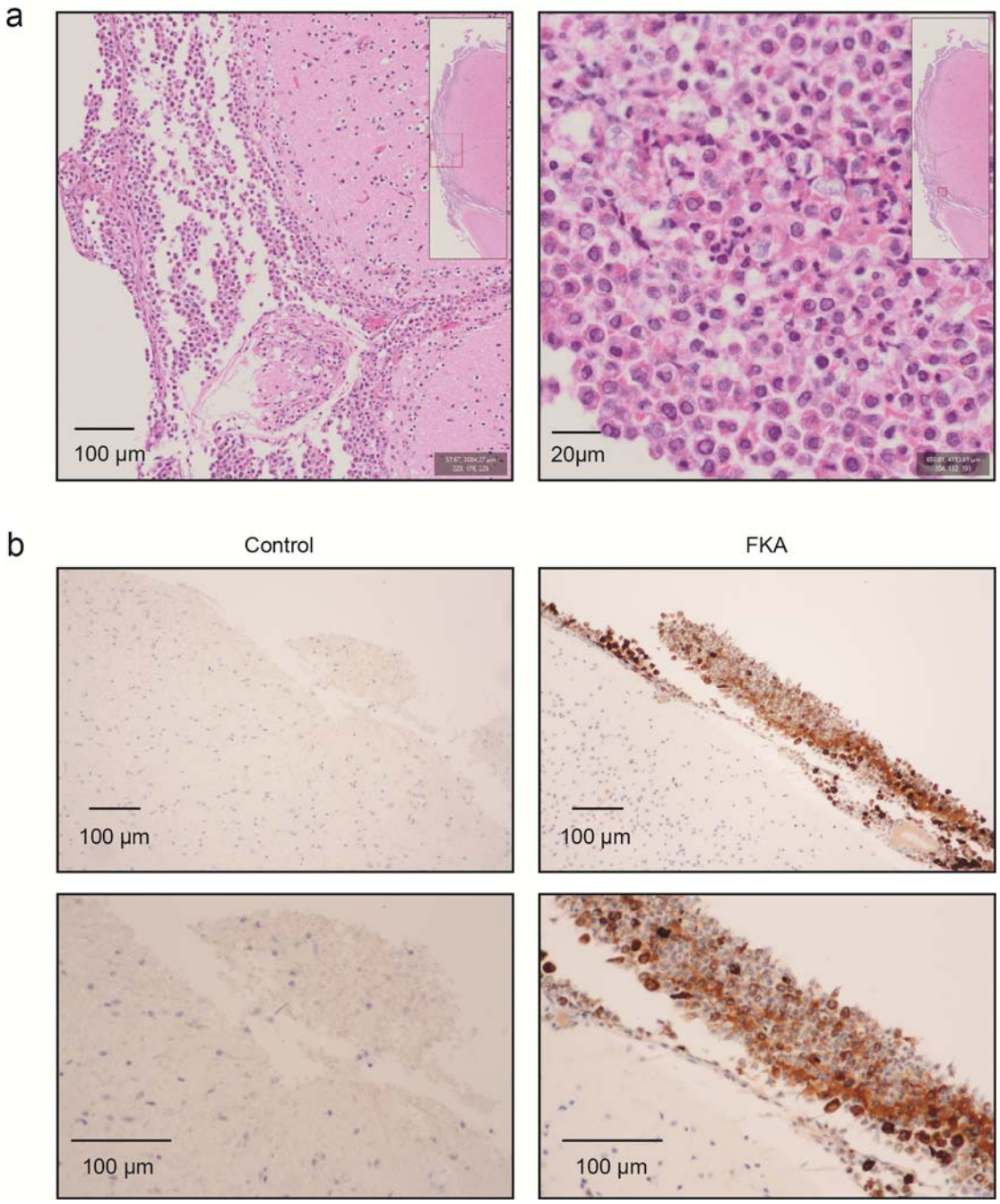

968

969 **Supplementary Figure 9. Myeloid cells in the leptomeninges of FKA mice.**

970 **a**, Representative hematoxylin and eosin stains performed on brain sections of FKA mice with neurologic
971 signs at endpoint. **b**, Myeloperoxidase stains performed on brain sections of a wild-type NRG-3GS mouse
972 and an FKA mouse, showing myeloid cell infiltration.

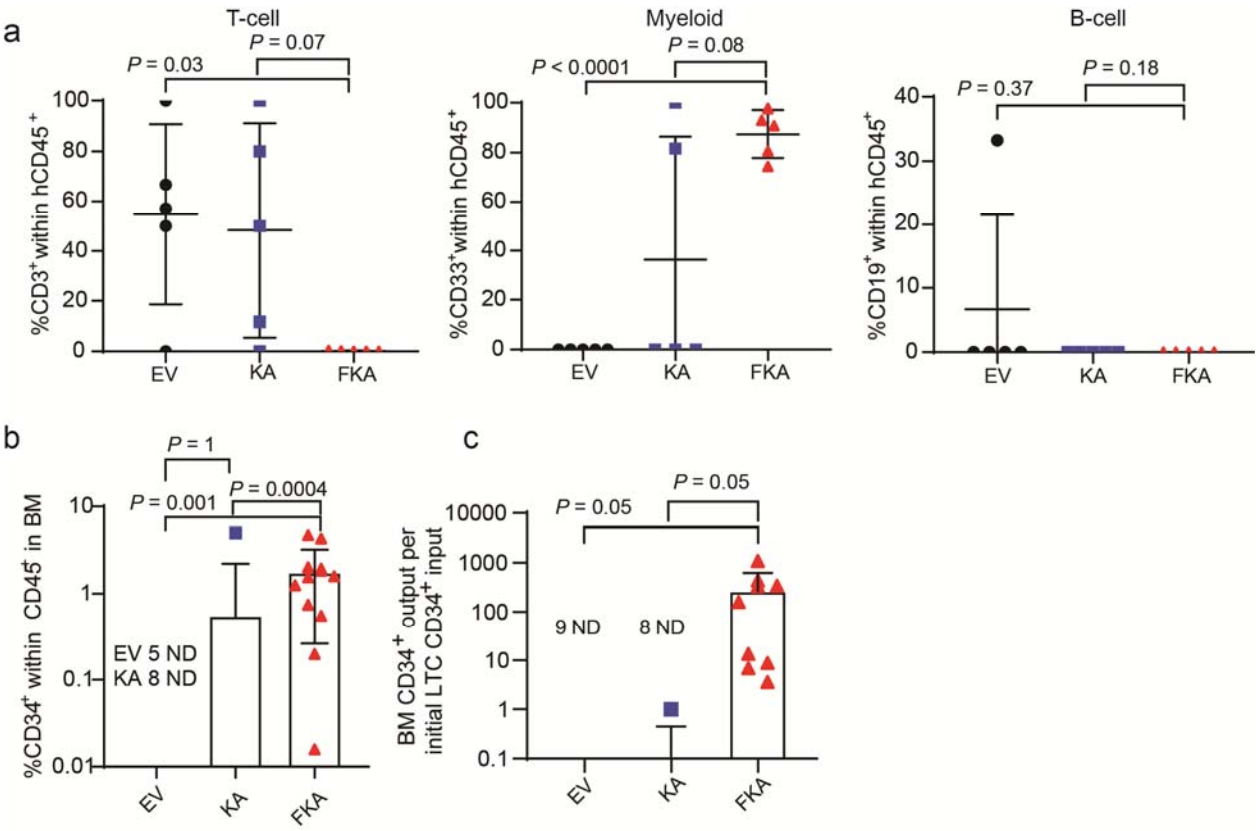

Supplementary Figure 10. Flow cytometry analysis of bone marrow cells harvested at endpoint. **a**, Flow cytometry analysis of lymphoid and myeloid cell engraftment at endpoint following xenotransplantion (*n* = 5 mice). *P* values represent two-tailed *t*-tests and error bars represent s.d. **b**, Percentages of CD34$^+$HSPC within the engrafted human hematopoietic cell population at endpoint (*n* = 5-12 mice, ND = not detected for values < 0.01%, *P* values represent Fisher's exact test). **c**, Numbers of CD34$^+$ cells generated at xenotransplant endpoint per input CD34$^+$ cell seeded into long-term culture (*n* = 9 mice, *P* values represent two-tailed *t*-tests). Error bars represent s.d.

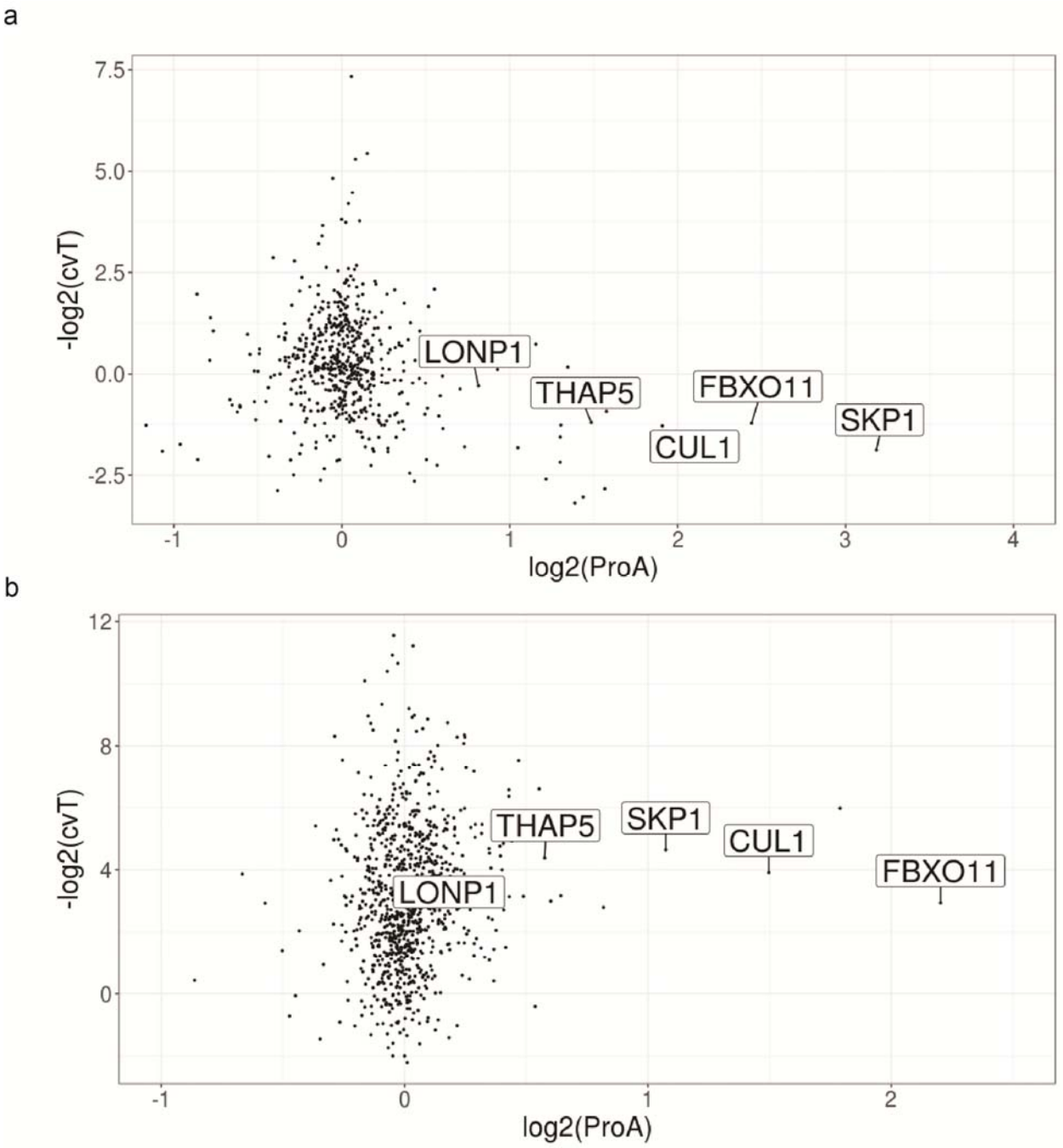

Supplementary Figure 11. Proteins co-immunoprecipitating with FLAG-FBXO11.
Mean protein abundance (log_2(ProA)) between replicates and transformed coefficient of variation (cvT) of FLAG-FBXO11 co-immunoprecipitated proteins **a**, without Benzonase® (*n* = 3 independent replicates) and **b**, with Benzonase® (*n* = 4 independent replicates), detected by quantitative tandem mass spectrometry. All detected proteins are plotted with the targets detected in both experiments labelled.

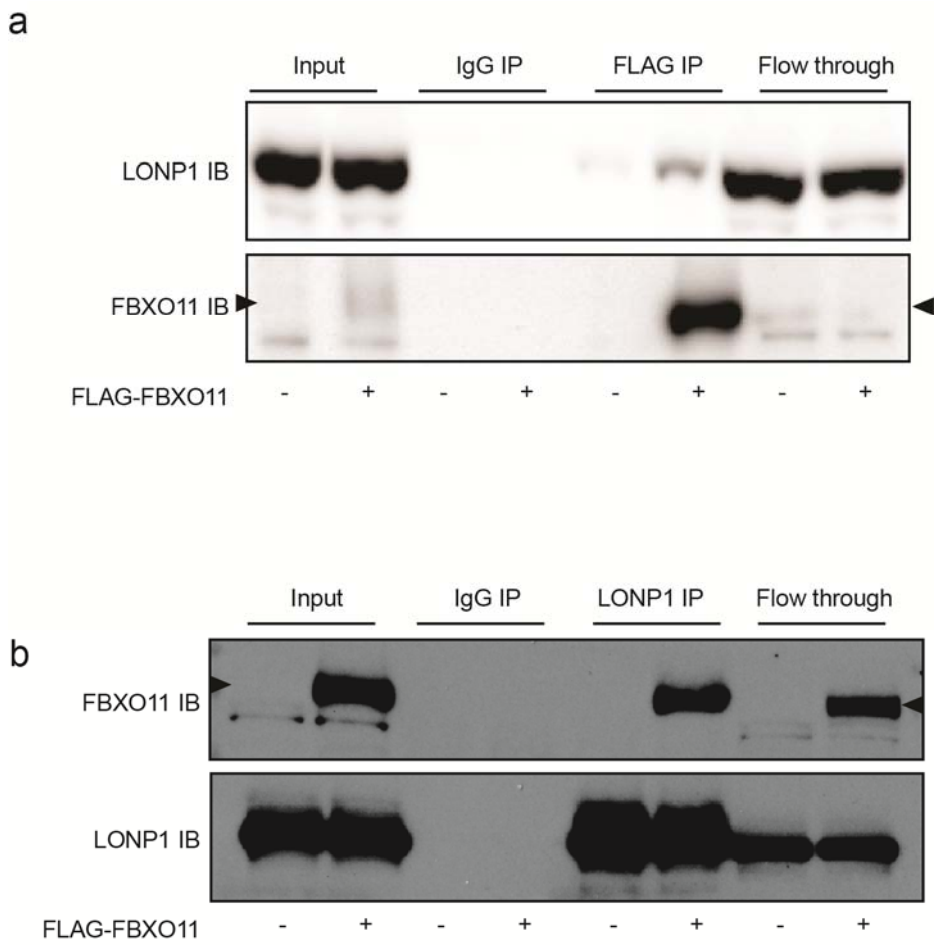

987

988 **Supplementary Figure 12. LONP1 co-immunoprecipitates with FBXO11.**
989 Co-immunoprecipitation (IP) with **a**, FLAG IP for FLAG-FBXO11 or **b**, LONP1 in *FBXO11* CRISPR KO K562
990 cells expressing empty vector (-) or FLAG-FBXO11 (+) followed by immunoblotting (IB) for LONP1 and
991 FBXO11.

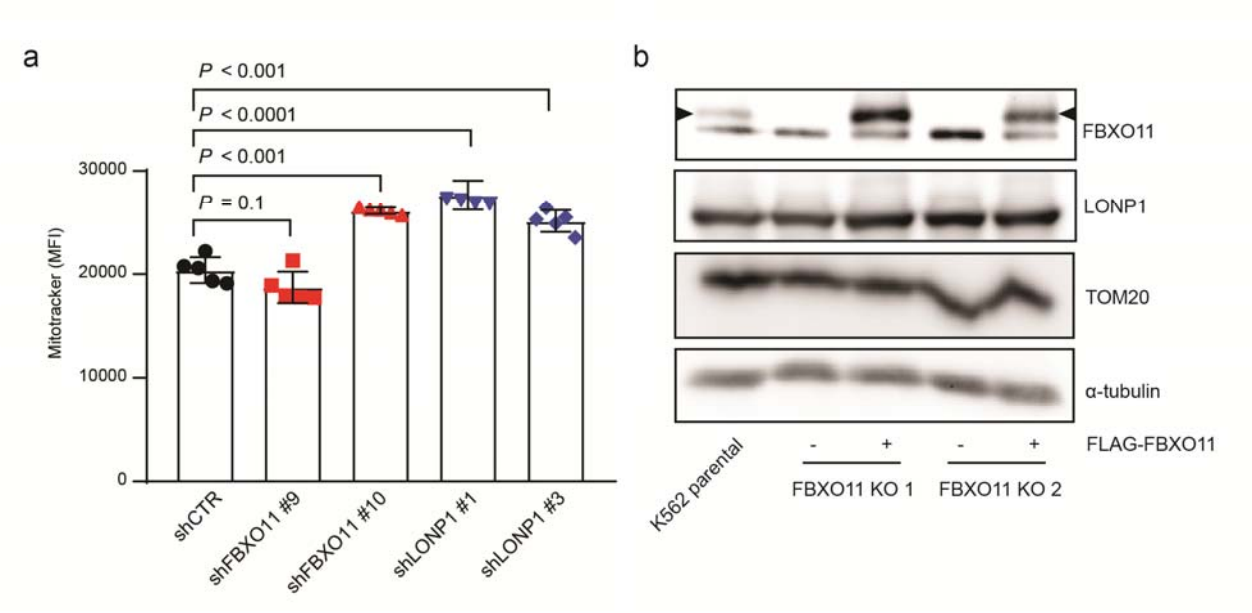

992

993 **Supplementary Figure 13. Mitochondrial mass does not decrease with *FBXO11* or *LONP1* knockdown.**
994 **a**, Mitochondrial mass of CD34$^+$ HSPC expressing control shRNA or shRNA targeting *FBXO11* or *LONP1*
995 was measured using detection of the Mitotracker dye by flow cytometry (n = 5), P values represent two-
996 tailed t-tests and error bars represent s.d **b**, Whole cell lysates from K562 parental cells (K562) or
997 *FBXO11* KO CRISPR clones (1-20 or 1-48) expressing empty vector (EV) or FLAG-FBXO11 (FBXO11) were
998 immunoblotted for TOM20.

999

1000

1001

1002

1003

1004

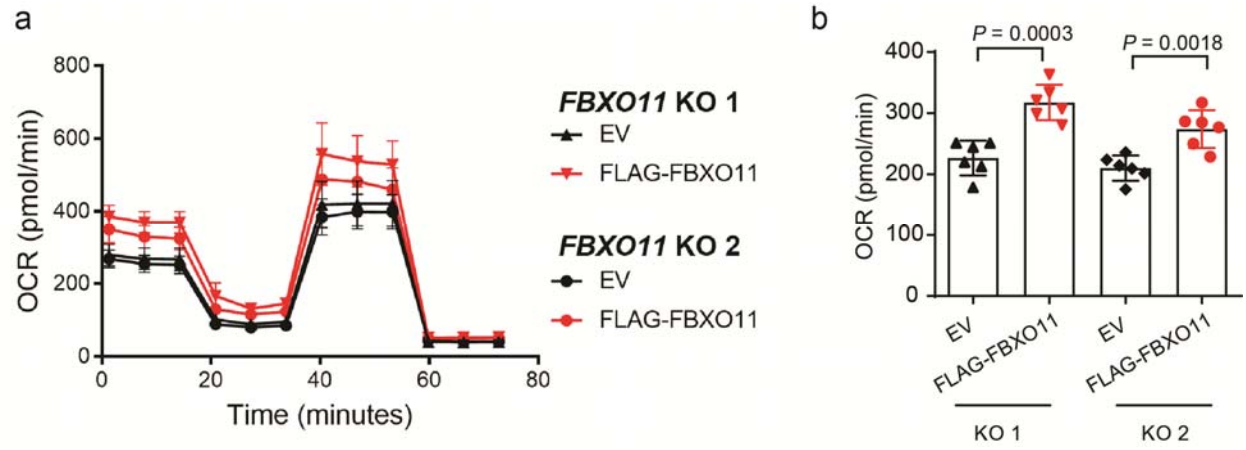

1005 **Supplementary Figure 14. *FBXO11* depletion reduces basal respiration.**
1006 **a**, Oxygen consumption rate (OCR) measured by the Agilent Seahorse XF Cell Mito Stress Test in K562
1007 *FBXO11* KO cells expressing empty vector (EV) or FLAG-FBXO11. Oligomycin was added at 20 min, FCCP
1008 at 40 min, and rotenone and antimycin A at 60 min according to the manufacturer's protocol. **b**,
1009 Quantification of basal respiration in K562 *FBXO11* KO cells expressing empty vector (EV) or FLAG-
1010 FBXO11 (n = 6 independent replicates, P values represent two-tailed t-tests, error bars represent s.d.).

1011

1012

1013

1014

1015

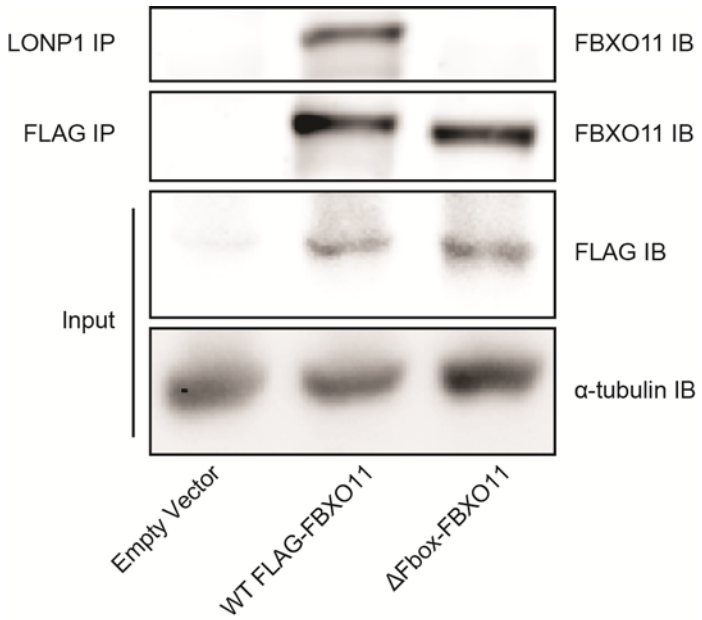

1016

1017 **Supplementary Figure 15. ΔFbox-FBXO11 does not interact with LONP1.**

1018 Lysate from K562 *FBXO11* KO cells expressing empty vector, WT FLAG-FBXO11, or ΔFbox-FBXO11

1019 immunoprecipitated with LONP1 or FLAG-tag antibody were immunoblotted for FBXO11.

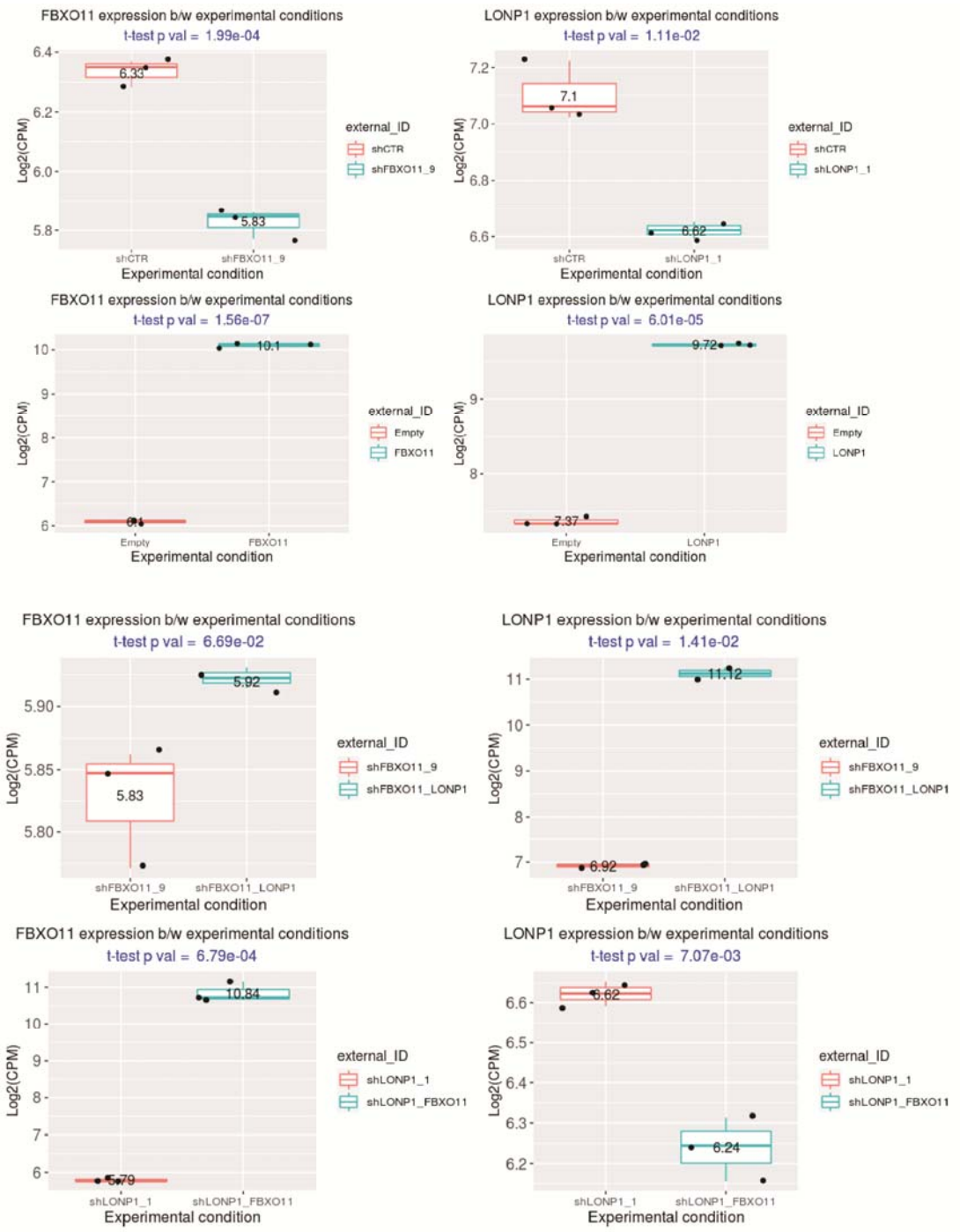

Supplementary Figure 16. Confirmation of *FBXO11* and *LONP1* transcript over-expression and/or knockdown in RNA-seq analysis.

Transcript expression of indicated genes expressed as $\log_2$(CPM) (counts per million reads mapped) between (b/w) indicated experimental conditions in CD34$^+$ HSPC RNA-seq experiment.

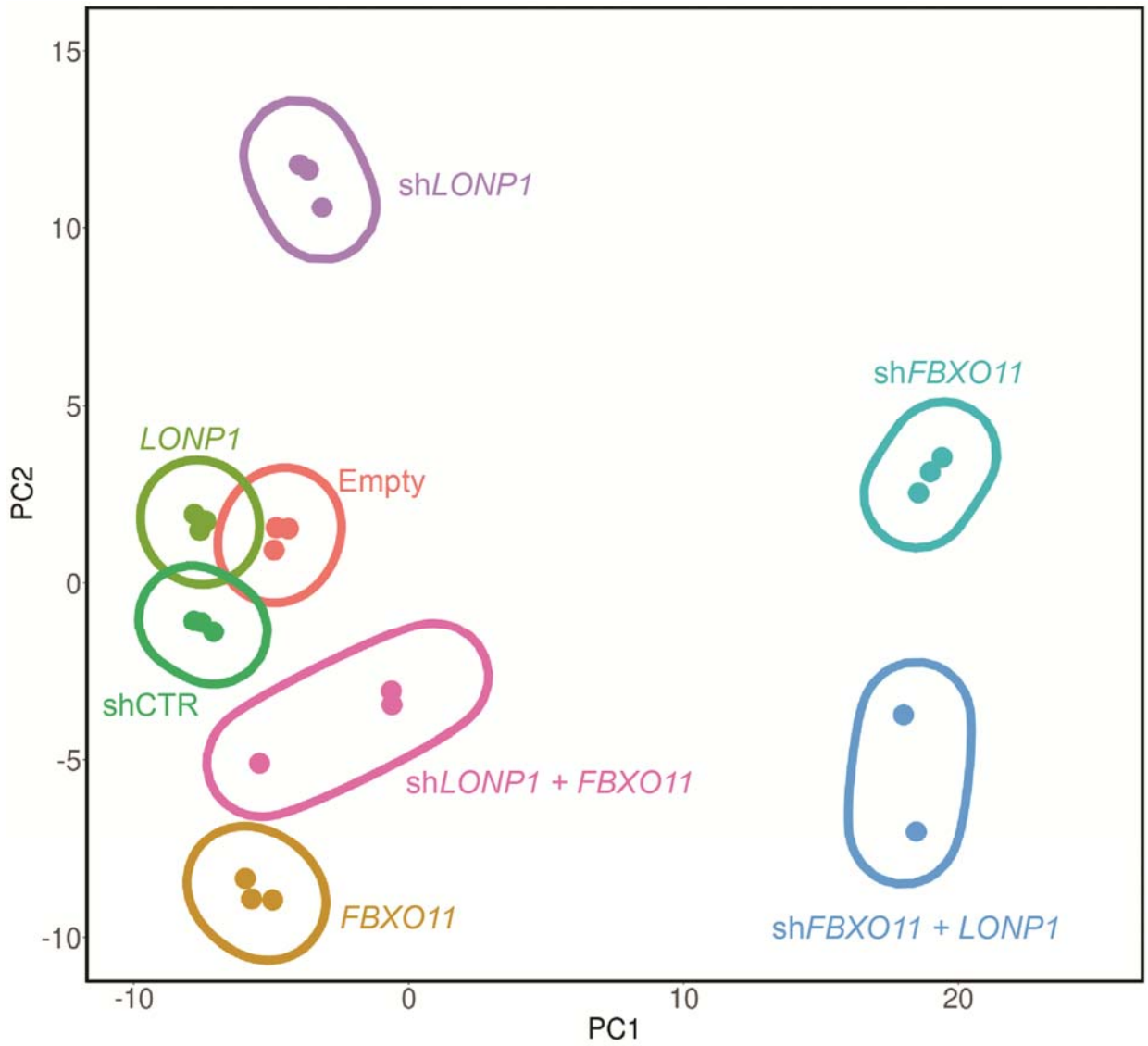

1027
1028
1029 **Supplementary Figure 17. Samples with enforced *LONP1* expression cluster with controls based on**
1030 **principal component analysis (PCA).**
1031 PCA projection of CD34$^+$ HSPC RNA-seq samples based on top 500 genes with the most variance
1032 between samples.
1033

gene	Bonferroni	AML	CD34pos	log2ratio
BTRC	1	6.383786	6.674664	-0.06428
CCNF	0.025837	6.468472	6.971789	-0.1081
CDRT1	0.00058	5.681126	5.248434	0.11429
CUL1	0.101034	8.421695	8.722577	-0.05064
CUL2	0.001001	6.269115	6.975092	-0.15395
CUL3	0.000464	10.23819	10.55676	-0.04421
CUL4A	7.29E-07	8.839108	9.445184	-0.09568
CUL4B	0.280942	8.406734	8.695217	-0.04868
CUL5	1	7.932351	7.782445	0.027525
CUL9	1	7.273609	7.314449	-0.00808
FBXL12	0.00837	7.545914	7.004289	0.107457
FBXL13	1	4.234858	4.052012	0.063675
FBXL14	0.598418	8.22075	8.446829	-0.03914
FBXL15	0.021766	4.619871	5.022584	-0.12058
FBXL16	1	4.249647	4.146436	0.035471
FBXL17	1	5.849973	6.137328	-0.06918
FBXL18	0.225488	6.829874	6.514919	0.068112
FBXL2	0.332631	4.075087	3.71212	0.134588
FBXL20	0.027861	6.718219	7.313227	-0.12243
FBXL21	0.641829	3.197972	3.019044	0.083066
FBXL22	0.517063	3.009556	2.763345	0.123135
FBXL3	1	8.604897	8.502053	0.017347
FBXL4	0.011047	5.733558	6.258962	-0.12649
FBXL5	0.006266	8.8741	8.493581	0.063228
FBXL6	0.010611	5.64689	5.191554	0.12129
FBXL7	0.211778	4.077939	3.825322	0.092259
FBXL8	0.081872	4.638568	4.294838	0.111076
FBXO10	1	5.286647	5.088592	0.055086
FBXO11	1.98E-20	8.450217	10.16896	-0.26711
FBXO15	1	3.708232	4.020797	-0.11675
FBXO16	1	3.097061	3.205479	-0.04964
FBXO18	0.651023	6.481602	6.930037	-0.09651
FBXO2	8.91E-09	5.593604	5.066621	0.142754
FBXO21	1.45E-13	5.566376	7.110985	-0.35331
FBXO22	4.17E-09	5.942976	7.192283	-0.27526
FBXO24	0.000497	5.373304	4.936751	0.122248
FBXO25	0.103737	5.946539	6.370584	-0.09938
FBXO27	0.000684	3.329626	2.911141	0.193776
FBXO28	0.00411	6.232379	6.905727	-0.14801
FBXO3	0.001604	7.701076	8.123975	-0.07713
FBXO30	1	5.899672	6.053246	-0.03707
FBXO31	0.062221	6.06403	6.915832	-0.18963
FBXO32	0.000297	4.708568	4.055171	0.215526
FBXO33	1	7.258648	7.14324	0.023122
FBXO34	7.97E-06	8.261786	8.712457	-0.07663
FBXO36	1	4.0747	4.047007	0.009839

FBXO38	0.15697	6.761349	7.291988	-0.109
FBXO39	1	3.235498	3.182729	0.023723
FBXO4	4.31E-14	5.327555	7.410196	-0.47604
FBXO40	0.00023	3.889987	3.499452	0.152637
FBXO41	1	7.707668	7.487921	0.041729
FBXO42	0.637248	6.386559	6.068334	0.073738
FBXO43	1	4.990368	5.176247	-0.05276
FBXO44	0.00025	5.744435	5.04373	0.187674
FBXO45	8.26E-05	7.120894	7.924449	-0.15425
FBXO46	9.75E-05	4.886537	5.419589	-0.14937
FBXO5	1	6.945466	6.927597	0.003717
FBXO6	0.007049	4.522667	3.75426	0.268645
FBXO7	1	9.561009	9.777294	-0.03227
FBXO8	0.002599	4.316951	5.029016	-0.22026
FBXO9	0.000936	9.661607	10.27134	-0.08829
FBXW10	1.18E-08	3.488457	2.636618	0.4039
FBXW11	1.53E-09	7.742311	8.479109	-0.13115
FBXW12	1	10.34142	10.29429	0.00659
FBXW2	0.255702	7.496454	7.865815	-0.06939
FBXW4	1	6.589137	6.399223	0.042193
FBXW4P1	4.15E-08	4.92105	4.09621	0.264677
FBXW5	0.220036	6.206805	5.75187	0.10982
FBXW7	0.966807	7.642473	7.924698	-0.05232
FBXW8	1	5.030357	4.989104	0.01188
FBXW9	1	5.211692	5.462585	-0.06783
KDM2A	0.098917	8.615216	8.893183	-0.04581
KDM2B	5.35E-05	8.737153	9.301857	-0.09036
SKP1	1.88E-12	11.07774	11.65312	-0.07305
SKP2	3.71E-10	8.074034	9.430684	-0.22407

Study of O	Sample ID	Cancer Typ	Cancer Typ	Protein Ch	Annotatior	Functional	Mutation T	Variant Ty	Count
Thyroid Ca	TCGA-FK-A3SD-01	Papillary Tl	Q156*	OncoKB: Li	MutationA	Nonsense_	SNP		1
Brain Lowe	TCGA-DB-A64U-01	Oligoastro	S915Cfs*7	OncoKB: Li	MutationA	Frame_Shi	DEL		1
Bladder Ur	TCGA-XF-AAMX-01	Bladder Ur	X852_splic	OncoKB: Li	MutationA	Splice_Site	SNP		1
Kidney Rer	TCGA-B0-5098-01	Renal Clea	A486Pfs*3	OncoKB: Li	MutationA	Frame_Shi	DEL		1
Kidney Rer	TCGA-B0-4712-01	Renal Clea	X816_splic	OncoKB: Li	MutationA	Splice_Reg	SNP		1
Uterine Co	TCGA-AX-A064-01	Uterine En	G511Efs*6	OncoKB: Li	MutationA	Frame_Shi	DEL		1
Uterine Co	TCGA-AJ-A5DW-01	Uterine En	R742*	OncoKB: Li	MutationA	Nonsense_	SNP		2
Uterine Co	TCGA-AX-A06F-01	Uterine En	E264*	OncoKB: Li	MutationA	Nonsense_	SNP		1
Uterine Co	TCGA-DF-A2KU-01	Uterine En	X420_splic	OncoKB: Li	MutationA	Splice_Site	SNP		1
Esophagea	TCGA-LN-A49N-01	Esophagea	D732Efs*3	OncoKB: Li	MutationA	Frame_Shi	INS		1
Skin Cutan	TCGA-DA-A1I1-06	Cutaneous	X780_splic	OncoKB: Li	MutationA	Splice_Site	SNP		1
Stomach A	TCGA-BR-A4QL-01	Stomach A	G435Wfs*	OncoKB: Li	MutationA	Frame_Shi	INS		1
Stomach A	TCGA-D7-A6EY-01	Tubular St	G619*	OncoKB: Li	MutationA	Nonsense_	SNP		1
Stomach A	TCGA-RD-A8NB-01	Diffuse Typ	X743_splic	OncoKB: Li	MutationA	Splice_Reg	SNP		1
Stomach A	TCGA-VQ-A8PT-01	Intestinal T	L895Vfs*2	OncoKB: Li	MutationA	Frame_Shi	DEL		1
Breast Inva	TCGA-D8-A1XK-01	Breast Inva	E608*	OncoKB: Li	MutationA	Nonsense_	SNP		1
Breast Inva	TCGA-D8-A27V-01	Breast Inva	F797Lfs*1	OncoKB: Li	MutationA	Frame_Shi	DEL		1
Colorectal	TCGA-A6-2686-01	Colon Ade	F332Lfs*1	OncoKB: Li	MutationA	Frame_Shi	DEL		1
Colorectal	TCGA-A6-5661-01	Colon Ade	D318Kfs*3	OncoKB: Li	MutationA	Frame_Shi	DEL		1
Head and I	TCGA-CV-5441-01	Head and I	C390Mfs*	OncoKB: Li	MutationA	Frame_Shi	INS		1
Head and I	TCGA-CN-5364-01	Head and I	T906Lfs*1	OncoKB: Li	MutationA	Frame_Shi	INS		1
Head and I	TCGA-F7-A624-01	Head and I	X120_splic	OncoKB: Li	MutationA	Splice_Reg	SNP		1
Cervical Sq	TCGA-JW-A5VL-01	Cervical Sq	S532*	OncoKB: Li	MutationA	Nonsense_	SNP		1
Cervical Sq	TCGA-EA-A410-01	Cervical Sq	E303Lfs*7	OncoKB: Li	MutationA	Frame_Shi	INS		1
Cervical Sq	TCGA-EA-A410-01	Cervical Sq	G573*	OncoKB: Li	MutationA	Nonsense_	SNP		1
Prostate A	TCGA-VP-A87D-01	Prostate A	FBXO11-IN	OncoKB: Li	MutationA	fusion	FUSION		1
Cholangioc	TCGA-4G-AAZO-01	Intrahepat	CLASP1-FB	OncoKB: Li	MutationA	fusion	FUSION		1
Breast Inva	TCGA-A7-A13D-01	Breast Inva	NEBL-FBXC	OncoKB: Li	MutationA	fusion	FUSION		1
Thyroid Ca	TCGA-DO-A2HM-01	Papillary Tl	R677T	OncoKB: U	MutationA	Missense_	SNP		1
Brain Lowe	TCGA-VW-A7QS-01	Oligodendr	I704K	OncoKB: U	MutationA	Missense_	SNP		1
Ovarian Se	TCGA-09-1675-01	Serous Ova	H252R	OncoKB: U	MutationA	Missense_	SNP		1
Ovarian Se	TCGA-09-2051-01	Serous Ova	G503E	OncoKB: U	MutationA	Missense_	SNP		1
Ovarian Se	TCGA-13-0800-01	Serous Ova	E827Q	OncoKB: U	MutationA	Missense_	SNP		1
Glioblastor	TCGA-06-5416-01	Glioblastor	D717Y	OncoKB: U	MutationA	Missense_	SNP		1
Glioblastor	TCGA-06-5416-01	Glioblastor	L106I	OncoKB: U	MutationA	Missense_	SNP		1
Sarcoma (T	TCGA-K1-A6RT-01	Leiomyosa	D161G	OncoKB: U	MutationA	Missense_	SNP		1
Lung Squa	TCGA-18-3416-01	Lung Squa	S694F	OncoKB: U	MutationA	Missense_	SNP		1
Lung Squa	TCGA-18-3417-01	Lung Squa	I366F	OncoKB: U	MutationA	Missense_	SNP		1
Lung Squa	TCGA-37-4141-01	Lung Squa	M210V	OncoKB: U	MutationA	Missense_	SNP		1
Lung Squa	TCGA-60-2698-01	Lung Squa	E365K	OncoKB: U	MutationA	Missense_	SNP		1
Lung Squa	TCGA-60-2703-01	Lung Squa	I737L	OncoKB: U	MutationA	Missense_	SNP		1
Lung Squa	TCGA-60-2719-01	Lung Squa	I864V	OncoKB: U	MutationA	Missense_	SNP		1
Lung Squa	TCGA-68-8251-01	Lung Squa	G504E	OncoKB: U	MutationA	Missense_	SNP		1
Lung Squa	TCGA-77-8131-01	Lung Squa	F348I	OncoKB: U	MutationA	Missense_	SNP		1
Lung Squa	TCGA-MF-A522-01	Lung Squa	G412E	OncoKB: U	MutationA	Missense_	SNP		1
Lung Squa	TCGA-NC-A5HI-01	Lung Squa	D270N	OncoKB: U	MutationA	Missense_	SNP		1

Lung Squa	TCGA-46-3767-01	Lung Squa	P674T	OncoKB: U	MutationA Missense_	SNP	1
Lung Squa	TCGA-52-7811-01	Lung Squa	D749N	OncoKB: U	MutationA Missense_	SNP	1
Bladder Ur	TCGA-FD-A6TB-01	Bladder Ur	E227K	OncoKB: U	MutationA Missense_	SNP	1
Bladder Ur	TCGA-FD-A3N5-01	Bladder Ur	D285N	OncoKB: U	MutationA Missense_	SNP	1
Bladder Ur	TCGA-XF-AAMQ-01	Bladder Ur	R263K	OncoKB: U	MutationA Missense_	SNP	1
Bladder Ur	TCGA-DK-A6AW-01	Bladder Ur	R861Q	OncoKB: U	MutationA Missense_	SNP	1
Bladder Ur	TCGA-E7-A85H-01	Bladder Ur	E483V	OncoKB: U	MutationA Missense_	SNP	1
Liver Hepa	TCGA-DD-AAD2-01	Hepatocell	Q50P	OncoKB: U	MutationA Missense_	SNP	2
Kidney Rer	TCGA-CJ-4916-01	Renal Clea	D175G	OncoKB: U	MutationA Missense_	SNP	1
Thymoma	TCGA-XM-A8RC-01	Thymoma	S831R	OncoKB: U	MutationA Missense_	SNP	1
Uterine Co	TCGA-AX-A1CE-01	Uterine En	A432V	OncoKB: U	MutationA Missense_	SNP	2
Uterine Co	TCGA-A5-A2K5-01	Uterine En	R102C	OncoKB: U	MutationA Missense_	SNP	1
Uterine Co	TCGA-AP-A059-01	Uterine En	A825D	OncoKB: U	MutationA Missense_	SNP	1
Uterine Co	TCGA-AP-A0LM-01	Uterine En	P898H	OncoKB: U	MutationA Missense_	SNP	1
Uterine Co	TCGA-AX-A05Z-01	Uterine En	A902S	OncoKB: U	MutationA Missense_	SNP	1
Uterine Co	TCGA-AX-A05Z-01	Uterine En	F805L	OncoKB: U	MutationA Missense_	SNP	1
Uterine Co	TCGA-AX-A060-01	Uterine En	N222D	OncoKB: U	MutationA Missense_	SNP	1
Uterine Co	TCGA-B5-A0K2-01	Uterine En	R133P	OncoKB: U	MutationA Missense_	SNP	1
Uterine Co	TCGA-B5-A11E-01	Uterine En	S328A	OncoKB: U	MutationA Missense_	SNP	1
Uterine Co	TCGA-BS-A0UF-01	Uterine En	F645C	OncoKB: U	MutationA Missense_	SNP	1
Uterine Co	TCGA-A5-A2K7-01	Uterine En	I436V	OncoKB: U	MutationA Missense_	SNP	1
Uterine Co	TCGA-AJ-A3QS-01	Uterine Se	G893E	OncoKB: U	MutationA Missense_	SNP	1
Uterine Co	TCGA-AX-A060-01	Uterine En	L189P	OncoKB: U	MutationA Missense_	SNP	1
Uterine Co	TCGA-AX-A06F-01	Uterine En	R885K	OncoKB: U	MutationA Missense_	SNP	1
Uterine Co	TCGA-AX-A06F-01	Uterine En	A754D	OncoKB: U	MutationA Missense_	SNP	1
Uterine Co	TCGA-AX-A06F-01	Uterine En	A112V	OncoKB: U	MutationA Missense_	SNP	1
Uterine Co	TCGA-AX-A1CE-01	Uterine En	C472Y	OncoKB: U	MutationA Missense_	SNP	1
Uterine Co	TCGA-B5-A1MX-01	Uterine En	G687C	OncoKB: U	MutationA Missense_	SNP	1
Uterine Co	TCGA-B5-A3FA-01	Uterine En	A710D	OncoKB: U	MutationA Missense_	SNP	1
Uterine Co	TCGA-B5-A3FC-01	Uterine En	A486V	OncoKB: U	MutationA Missense_	SNP	1
Uterine Co	TCGA-DF-A2KN-01	Uterine En	R742Q	OncoKB: U	MutationA Missense_	SNP	1
Uterine Co	TCGA-EO-A3B0-01	Uterine En	I566M	OncoKB: U	MutationA Missense_	SNP	1
Lung Aden	TCGA-44-A47G-01	Lung Aden	C495S	OncoKB: U	MutationA Missense_	SNP	1
Lung Aden	TCGA-49-AAR9-01	Lung Aden	S292F	OncoKB: U	MutationA Missense_	SNP	1
Lung Aden	TCGA-50-6593-01	Lung Aden	D192V	OncoKB: U	MutationA Missense_	SNP	1
Lung Aden	TCGA-55-7907-01	Lung Aden	Y468F	OncoKB: U	MutationA Missense_	SNP	1
Lung Aden	TCGA-86-8073-01	Lung Aden	K246M	OncoKB: U	MutationA Missense_	SNP	1
Lung Aden	TCGA-17-Z055-01	Lung Aden	N349Y	OncoKB: U	MutationA Missense_	SNP	1
Lung Aden	TCGA-MP-A4TI-01	Lung Aden	G550A	OncoKB: U	MutationA Missense_	SNP	1
Skin Cutan	TCGA-EE-A29Q-06	Cutaneous	P582L	OncoKB: U	MutationA Missense_	SNP	1
Skin Cutan	TCGA-EE-A2MR-06	Cutaneous	P108L	OncoKB: U	MutationA Missense_	SNP	1
Skin Cutan	TCGA-EE-A20C-06	Cutaneous	N817I	OncoKB: U	MutationA Missense_	SNP	1
Skin Cutan	TCGA-D9-A6EC-06	Cutaneous	K715T	OncoKB: U	MutationA Missense_	SNP	1
Skin Cutan	TCGA-DA-A1IA-06	Cutaneous	S169F	OncoKB: U	MutationA Missense_	SNP	1
Skin Cutan	TCGA-D3-A2JD-06	Cutaneous	M466I	OncoKB: U	MutationA Missense_	SNP	1
Skin Cutan	TCGA-D3-A2JP-06	Cutaneous	G757C	OncoKB: U	MutationA Missense_	SNP	1
Skin Cutan	TCGA-D3-A2JP-06	Cutaneous	G513V	OncoKB: U	MutationA Missense_	SNP	1

Skin Cutan	TCGA-D9-A1X3-06	Cutaneous	G500V	OncoKB: U	Mutation	A Missense_	SNP	1
Skin Cutan	TCGA-EB-A24C-01	Cutaneous	G596W	OncoKB: U	Mutation	A Missense_	SNP	1
Skin Cutan	TCGA-FS-A1Z0-06	Cutaneous	P193Q	OncoKB: U	Mutation	A Missense_	SNP	1
Skin Cutan	TCGA-FS-A1ZB-06	Cutaneous	R852I	OncoKB: U	Mutation	A Missense_	SNP	1
Stomach A	TCGA-BR-8372-01	Stomach A	Y913C	OncoKB: U	Mutation	A Missense_	SNP	1
Stomach A	TCGA-BR-4362-01	Stomach A	K602R	OncoKB: U	Mutation	A Missense_	SNP	1
Stomach A	TCGA-BR-6452-01	Stomach A	V643I	OncoKB: U	Mutation	A Missense_	SNP	1
Stomach A	TCGA-BR-6802-01	Stomach A	S626N	OncoKB: U	Mutation	A Missense_	SNP	1
Stomach A	TCGA-BR-7715-01	Stomach A	T894I	OncoKB: U	Mutation	A Missense_	SNP	1
Stomach A	TCGA-CD-A4MG-01	Diffuse Typ	V528A	OncoKB: U	Mutation	A Missense_	SNP	1
Stomach A	TCGA-CG-5733-01	Intestinal T	E904G	OncoKB: U	Mutation	A Missense_	SNP	1
Stomach A	TCGA-HU-8602-01	Diffuse Typ	T491A	OncoKB: U	Mutation	A Missense_	SNP	1
Stomach A	TCGA-R5-A7ZI-01	Diffuse Typ	A754T	OncoKB: U	Mutation	A Missense_	SNP	1
Stomach A	TCGA-VQ-A8PT-01	Intestinal T	N523S	OncoKB: U	Mutation	A Missense_	SNP	1
Breast Inva	TCGA-A2-A04X-01	Breast Inva	D591N	OncoKB: U	Mutation	A Missense_	SNP	1
Breast Inva	TCGA-D8-A27P-01	Breast Inva	N564S	OncoKB: U	Mutation	A Missense_	SNP	1
Breast Inva	TCGA-A2-A25A-01	Breast Inva	P82T	OncoKB: U	Mutation	A Missense_	SNP	1
Breast Inva	TCGA-E2-A150-01	Breast Inva	I864L	OncoKB: U	Mutation	A Missense_	SNP	1
Pancreatic	TCGA-IB-7651-01	Pancreatic	F777L	OncoKB: U	Mutation	A Missense_	SNP	1
Pancreatic	TCGA-XD-AAUI-01	Pancreatic	R185H	OncoKB: U	Mutation	A Missense_	SNP	1
Colorectal	TCGA-AG-3892-01	Rectal Ade	F850L	OncoKB: U	Mutation	A Missense_	SNP	1
Colorectal	TCGA-AA-3667-01	Colon Ade	T616S	OncoKB: U	Mutation	A Missense_	SNP	1
Colorectal	TCGA-AA-3845-01	Colon Ade	A787T	OncoKB: U	Mutation	A Missense_	SNP	2
Colorectal	TCGA-AA-3845-01	Colon Ade	A432V	OncoKB: U	Mutation	A Missense_	SNP	2
Colorectal	TCGA-WS-AB45-01	Mucinous	Q50P	OncoKB: U	Mutation	A Missense_	SNP	2
Colorectal	TCGA-DC-4749-01	Rectal Ade	R185C	OncoKB: U	Mutation	A Missense_	SNP	1
Colorectal	TCGA-F5-6814-01	Rectal Ade	S626I	OncoKB: U	Mutation	A Missense_	SNP	1
Colorectal	TCGA-AD-6895-01	Colon Ade	Q220R	OncoKB: U	Mutation	A Missense_	SNP	1
Colorectal	TCGA-D5-6540-01	Mucinous	A83V	OncoKB: U	Mutation	A Missense_	SNP	1
Colorectal	TCGA-D5-6924-01	Colon Ade	N489S	OncoKB: U	Mutation	A Missense_	SNP	1
Colorectal	TCGA-F4-6856-01	Mucinous	Q667R	OncoKB: U	Mutation	A Missense_	SNP	1
Colorectal	TCGA-G4-6304-01	Colon Ade	R380Q	OncoKB: U	Mutation	A Missense_	SNP	1
Colorectal	TCGA-G4-6304-01	Colon Ade	T207I	OncoKB: U	Mutation	A Missense_	SNP	1
Colorectal	TCGA-NH-A6GB-01	Colon Ade	G603E	OncoKB: U	Mutation	A Missense_	SNP	1
Kidney Ren	TCGA-IA-A83V-01	Papillary R	R723I	OncoKB: U	Mutation	A Missense_	SNP	1
Kidney Ren	TCGA-A4-8630-01	Papillary R	N541K	OncoKB: U	Mutation	A Missense_	SNP	1
Kidney Ren	TCGA-MH-A561-01	Papillary R	G688E	OncoKB: U	Mutation	A Missense_	SNP	1
Kidney Ren	TCGA-KV-A6GE-01	Papillary R	V4L	OncoKB: U	Mutation	A Missense_	SNP	1
Head and I	TCGA-BA-5152-01	Head and I	M211I	OncoKB: U	Mutation	A Missense_	SNP	1
Head and I	TCGA-CV-7416-01	Head and I	V182I	OncoKB: U	Mutation	A Missense_	SNP	1
Head and I	TCGA-WA-A7GZ-01	Head and I	R448W	OncoKB: U	Mutation	A Missense_	SNP	1
Head and I	TCGA-CN-6010-01	Head and I	M201I	OncoKB: U	Mutation	A Missense_	SNP	1
Cervical Sq	TCGA-EA-A3HU-01	Cervical Sq	A787T	OncoKB: U	Mutation	A Missense_	SNP	2
Cervical Sq	TCGA-EK-A2RJ-01	Cervical Sq	R731T	OncoKB: U	Mutation	A Missense_	SNP	1
Cervical Sq	TCGA-FU-A3NI-01	Cervical Sq	R448Q	OncoKB: U	Mutation	A Missense_	SNP	1
Cervical Sq	TCGA-FU-A3HZ-01	Cervical Sq	I366M	OncoKB: U	Mutation	A Missense_	SNP	1

	LTC		*In vivo*		BM CD34+ output per initial LTC CD34+ cell input	standard deviation
	Starting #CD34+ cells	#CD34+ cells at harvest	*In vivo* starting #CD34+ cells/mouse	#CD34+ cells at endpoint BM		
EV (9)	2500	13663	1500	1	0	0
KA (9)	2539	287168	23622	37	0	0
FKA (9)	2439	1161293	53558	675000	6001	350

Number of $CD34^+$ cells counted or calculated at each stage of the experiment from seeding cells for long

g-term culture to bone marrow cell harvest at xenotransplant endpoint.

Other (Translocations, Supp Fig. 1c)

Patient	Subtype	Gene	Type of alteration
79-85	AML	DEK,NUP214	Rearrangement/Translocation/Fusion
112-75	AML	SET/NUP214	Rearrangement/Translocation/Fusion
99-21	AML	CREBBP/MYST3	Rearrangement/Translocation/Fusion
104-89	AML	HOXA9:NUP98	Rearrangement/Translocation/Fusion
130-99	AML	MLLT10:PICALM	Rearrangement/Translocation/Fusion
123-46	AML	NUP98/NSD1	Rearrangement/Translocation/Fusion
166-86	tAML	NUP98,TOP1	Rearrangement/Translocation/Fusion

Other (Activated Signalling, Supp Fig. 1c)

Patient	Subtype	Gene	Type of alteration
147-27	AML	JAK2	Missense
108-24	AML	MAP2K5	Missense
93-60	AML	STK11	Missense
114-04	AML	PTPRT	Missense
130-00	AML	SMG	Missense
164-52	AML	CSF3R	Frameshift
203-06	AML	CSF3R	Missense
130-99	AML	BCR,ABL	Rearrangement/Translocation/Fusion
122-32	AML	TTBK1	Splice Site
77-71	sAML	MAP2K5	Missense

Other (Chromatin Modifiers, Supp Fig. 1c)

Patient	Subtype	Gene	Type of alteration
112-75	AML	SET	Missense
93-60	AML	KDM2B	Frameshift
93-60	AML	KAT6B	Missense
162-30	AML	BRWD3	Missense
124-05	AML	SMARCA4	Missense
130-99	AML	SETD1B	Nonsense
77-84	AML	KDM6A	Frameshift
208-80	sAML	KAT6B	Frameshift
96-26	tAML	SMYD4	Frameshift

Other (Activated Signalling, Fig. 1a)

Patient	Subtype	Gene	Type of alteration
147-27	AML	JAK2	Missense
108-24	AML	MAP2K5	Missense
13-00468	tAML	CSF3R	Missense

13-00557	AML	CSF3R	Missense
13-00625	AML	CSF3R	Truncating
14-00676	tAML	STK11	Missense
14-00738	tAML	JAK2	Missense
15-00171	AML	JAK2	Missense
15-00353	AML	JAK2	Missense
PASBBE	Ped AML	CSF3R	Missense

Mutation
DEK/NUP214
SET/NUP214
CREBBP/MYST3
HOXA9:NUP98
MLLT10:PICALM
NUP98/NSD1
NUP98:TOP1

Mutation
V617F
S133G
S404F
Y687C
G974D
Y814fs
P721L
BCR/ABL
E753E
Y145C

Mutation
S144F
FS
V1456I
G1153S
R1243W
R1286*
FS (CTGTT Insertion at chr12:122018732)
L1053_D1054fs
L57fs

Mutation	dataset
V617F	PMP
S133G	PMP
T618I	Beat AML

T618I	Beat AML
Q776*	Beat AML
L182R	Beat AML
V617F	Beat AML
R683S	Beat AML
V617F	Beat AML
T618I	Target